



Norwegian University of
Science and Technology

Binary VLE measurements and modeling for selected amine systems

Fahad Saleem

Chemical Engineering

Submission date: June 2011

Supervisor: Hallvard Fjøsne Svendsen, IKP

Acknowledgements

This masters' thesis was completed at the Department for Chemical Engineering at Norwegian University of Science & Technology (NTNU).

I would like to extend my deepest gratitude to my supervisor Professor Hallvard F. Svendsen for his kind guidance and help at every stage of this work without which I would never have been able to complete it. Then comes the turn of Dr. Ardi Hartono, whose eternal presence and availability made things easy for me during the whole period and whose help was also instrumental in the modeling part of this work. Special thanks for Dr. Inna Kim for her guidance in the operation of apparatus and for always finding time to answer my questions and whose earlier work in the same area served as a guiding light for me. Thanks to Sintef people also for letting me use their lab apparatuses especially for analyses of my samples.

Last but not the least I would like to dedicate my work to two mothers; one is mother earth; mother of us all, from where we all originate and to whom shall we all return one day and the second one is my own mother who is the reason of each & everything that I am today.

Abstract

Chemical absorption with amines is considered to be the most viable industrial process for the removal of acid gases from various gas streams. Such processes, although being very efficient in their performance, are usually associated with very large energy consumptions. A large portion (2.8–3.2 GJ/ton of recovered CO₂; as claimed by MHI and Fluor) of this energy is required in the solution regeneration step of the process. Most of the research these days is focused on making these processes more energy efficient thus making them economical enough to compensate for the increasing energy costs. Also, down the line, this would enable such processes to be used for CO₂ capture from flue gases which is the ultimate goal of this research area.

In order to improve the performance of absorption systems, deep understanding of the very basic properties such as VLE (Vapor liquid equilibria) is imperative. Accurate and reliable VLE data is necessary for thermodynamic modeling. For engineering purposes, it is often necessary to make estimates of the activity coefficients for mixtures, where only fragmentary data or no data at all, is available (Kim, 2009). During the course of this work, VLE data of pure and mixtures of DEEA & DIPEA with water was measured in a modified Świątosławski ebulliometer up to a maximum pressure of 1 bar and for a temperature range of 50 to 95°C. The data was used to calculate experimental activity coefficients for the liquid and vapor phases, which in turn can be used for testing VLE models on their ability to predict the system behavior at zero loading.

Fourier Transform Infrared (FTIR) spectroscopy is a very effective analyses technique which can give information about both the quality and quantity of any specie simultaneously. This technique was employed for amine analyses during the present work. Spectra of the samples from ebulliometer were produced in FTIR and the quantities of amine were predicted by using a ‘calibration model’ approach in a multivariate data analyses software: The Unscrambler. The results produced are very accurate and reliable and were used to calculate experimental activity coefficients.

The VLE data thus obtained was modeled using NRTL, Wilson and UNIQUAC models. The DEEA system gives very good fit but unfortunately DIPEA system could not be modeled properly due to the lack of vapor phase data (caused by immiscibility of DIPEA with water).

Table of Contents

1.0	Introduction	1
1.1	World's CO ₂ emissions scenario	1
1.2	CO ₂ removal techniques; an overview	2
1.2.1	Post Combustion CO ₂ capture	2
1.2.2	Pre-combustion CO ₂ capture	3
1.2.3	CO ₂ capture by Oxyfuel	4
1.3	Motivation & scope for the present work	5
2.0	Theoretical background	6
2.1	Thermodynamic framework for VLE	6
2.1.1	Fugacity & activity	7
2.1.2	Activity & activity coefficients	8
2.1.3	Standard & reference state	9
2.1.4	Normalization of activity coefficients	10
2.1.5	Excess functions	10
2.1.6	The Gibbs-Duhem equation	10
2.1.7	Modeling of data	11
2.1.8	Thermodynamic consistency of data	13
2.2	Fourier Transform Infrared (FTIR) spectroscopy	13
2.2.1	Introduction	13
2.2.2	Why FTIR?	14
2.2.3	How it works?	14
2.2.4	Interpreting the FTIR spectra	16

2.2.5	FTIR at NTNU; FLTA 2000-104	17
3.0	VLE measurements	19
3.1	Overview of present work	19
3.2	Experimental technique	19
3.3	Experimental Procedure	20
3.4	Analyses of liquid and vapor phase samples	21
3.5	Results and discussion	21
3.5.1	FTIR results	21
3.5.1.1	Discussion on FTIR results	22
3.6	Vapor pressure data of pure water	27
3.7	Vapor pressure data for pure DEEA and DIPEA	27
3.8	VLE of DEEA-H ₂ O solution	29
3.9	VLE of DIPEA-H ₂ O system	39
3.10	Probable sources of error	45
3.11	Proposed future work and recommendations	46

Conclusion

References

Appendices

1.0 Introduction

The main motivation of this work originates from one of the gravest problems facing our planet today namely, CO₂ emissions. Just to put everything in perspective the report starts with a brief overview of the major causes and effects of the said emissions and a brief overview of the techniques which could be employed to reduce these emissions.

1.1 World's CO₂ emission scenario; an overview:

Over the last few decades the issue of CO₂ emissions, due to its role in potential global warming, has become a major cause of concern for all industrialized nations. It is expected that if no new policies are implemented the CO₂ emissions will more than double by the year 2050 (24.5 GT in 2003 to 58 GT in 2050) (IEA, 2008). So there has been a lot of emphasis on cutting down these emissions. A study by United Nation's Intergovernmental Panel on Climate Change (IPCC) is shown in table 1. It indicates that there is a need to cut CO₂ emissions by 50%-85% from the level they were at in 2001 in order to keep the global mean temperature rise in the range of 2.0°C to 2.4°C by the year 2050.

Temperature increase (°C)	All GHGs (ppm CO ₂ equivalent)	CO ₂ (ppm CO ₂)	CO ₂ emissions 2050 (% of 2000 emissions)
2.0 - 2.4	445 - 490	350 - 400	-85 to -50
2.4 - 2.8	490 - 535	400 - 440	-60 to -30
2.8 - 3.2	535 - 590	440 - 485	-30 to +5
3.2 - 4.0	590 - 710	485 - 570	+10 to +60

Table 1.1: Relation between emissions & climate change (IPCC 2007 assessment report) [IEA, 2008]

CO ₂ emissions by sector	Emissions 2000 (Gt CO ₂)	Emissions 2005 (Gt CO ₂)	2000-2005 % Change
Electricity and heat production	8	9.6	19.6
Industry	6.3	6.8	7.1
Transport	5	5.2	3.8
Residential	1.9	2.2	18.2
Fuel transformation	0.7	0.9	43.1
Commercial	0.7	0.9	33.9
Agriculture	0.6	0.7	7.1
Total	23.2	26.3	13.4

Table 1.2: Evolution of CO₂ emission by sector (200-2005) [IEA, 2008]

The use of fossil fuel is the main source of world's CO₂ emissions. Table 2 shows sector wise distribution of world's CO₂ emissions sources. It can be clearly seen from the table that electricity and heat production are the biggest source of CO₂ emissions into the open atmosphere. If these emissions can be reduced somehow it would surely have a substantial impact on the overall scenario of CO₂ capture. Although a lot of effort has been put into making the process of CO₂ capture from power plants economically feasible but the fact of the matter is that the technology available to date is not mature enough to meet these cherished goals.

1.2 CO₂ Removal techniques; an overview

“Fundamentally, there are a number of ways to reduce the level of CO₂ emissions from fossil fuel usage:

- 1) Increasing the "fuel to end-use" energy conversion efficiency
- 2) Replacing high-carbon fuels with lower-carbon fuels
- 3) Capturing and storing, in suitable geological formations, the CO₂ emitted from fossil fuel energy conversion systems

While the first two are effective options, they alone cannot fully mitigate the global increase in CO₂ emissions. The third option de-couples the use of fossil fuels from CO₂ emissions, thus allowing for the continued use of fossil fuel in a sustainable way. Hence, immense opportunities exist for a significant reduction in greenhouse gas (GHG) emissions from industrial processes and power plants through the capture and storage of CO₂”.

Currently, there are three main approaches to capturing CO₂ from the fossil fuel energy conversion systems, namely, pre-combustion capture, post-combustion capture, and oxy-fuel combustion with CO₂ capture. A brief description of each is given below.

1.2.1 Post-combustion CO₂ capture

To reduce the existing emissions, post-combustion CO₂ capture can be used. The process is based on chemical absorption, where the flue gas is brought into contact with a chemical absorbent with an ability to attach the CO₂.

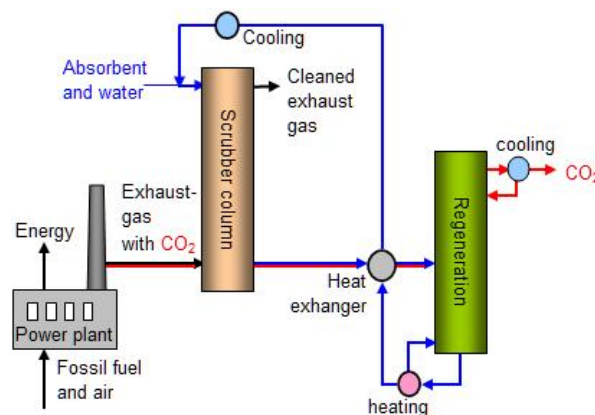


Fig1.1: Post combustion CO₂ capture ^[11]

This process continues inside a scrubber column. Scrubber column is designed to ensure that the exhaust gas and the absorbent are brought into close contact with each other. The CO₂ is then transferred from the flue gas to the absorbent, and there are two out-going flows from the scrubber column; a cleaned gas-stream with low CO₂ content and liquid-stream containing water, absorbent and CO₂.

After the absorption process, the absorbent and the CO₂ are separated in a regeneration column. When heated, the absorbents ability to retain CO₂ is reduced, resulting in regeneration of the absorbent, which can then be re-used. The CO₂ leaves the regeneration column as a gas stream of high CO₂ purity. This gas can be transported to a CO₂ storage site.

80 to 90 percent of the CO₂ from a power plant can typically be removed by post-combustion CO₂ capture. An advantage of post-combustion technology is that it can be added to an existing power plant without modifying the original power plant.

1.2.2 Pre-combustion CO₂ capture

CO₂ can be separated from the fossil fuel before combustion, the so-called pre-combustion CO₂ capture method.

The principle of this process is first to convert the fossil fuel into CO₂ and Hydrogen gas (H₂). Then, the H₂ and the CO₂ is separated in the same way as under post-combustion, however a smaller installation can be used. This results in a Hydrogen-rich gas which can be used in power plants or as fuel in vehicles. The combustion of Hydrogen does not lead to any creation of CO₂. The process is described in figure 1.2.

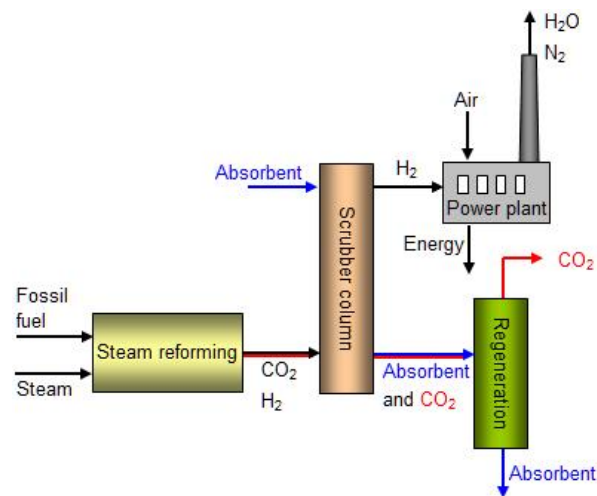


Fig1.2: Pre combustion CO₂ capture ^[1]

When using natural gas for power production, the natural gas and steam is converted into synthesis gas in a traditional steam reformer. Synthesis gas is a common industrial gas consisting of carbon mono-oxide (CO) and hydrogen gas. The CO subsequently reacts with steam to form CO₂.

The pre-combustion CO₂ capture is applicable to coal power plants and there is a lot of focus on the IGCC technology (Integrated coal Gasification Combined Cycle), where coal is converted into CO₂ and H₂ before combustion.

By pre-combustion CO₂ capture about 90 percent of the CO₂ from a power plant can be removed. As the technology requires significant modifications of the power plant, it is only viable for new power plants, not for existing plants.

Using today's technologies, the investment costs for a gas power plant with pre-combustion CO₂ capture will be twice as high as for a similar plant using post combustion of flue gas (Thomas, 2005). The separation of CO₂ from fossil fuel prior to combustion will become far more interesting as technological development will bring down investment- and operating costs.

1.2.3 CO₂ capture by 'Oxyfuel'

In traditional fossil fuelled power plants, combustion is carried out using air, where the nitrogen (N₂) in the air follows the flue gas. An alternative is to use pure oxygen (O₂) instead of air in the combustion. The advantage of this so-called oxyfuel technique is that the flue gas only contains steam and CO₂. These two components are easily separated through cooling. The water then condenses, and a CO₂ rich gas-stream is formed. Up to 100 percent CO₂ can be captured in this process which is illustrated in Figure 1.3.

The combustion of natural gas and pure oxygen gives high material stress in the gas turbine; hence the development of new materials is a prerequisite for deployment of this technology. In coal powered plants, this obstacle is avoided, as combustion is done in a boiler.

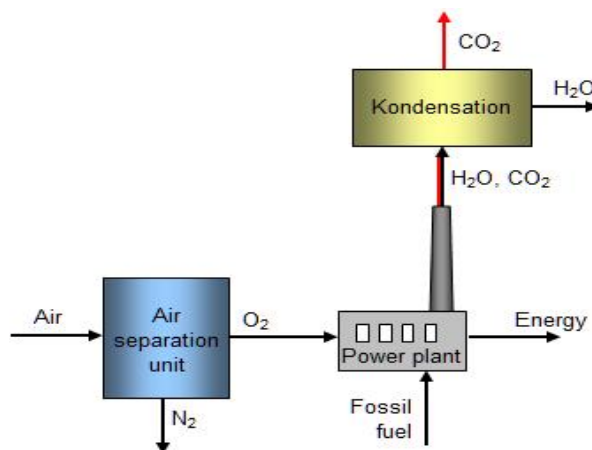


Fig1.3: CO₂ capture by Oxyfuel^[11]

The currently available technologies for pure oxygen-production are based primarily on cryogenic separation of air, where the air is cooled down below the boiling point before the liquefied oxygen, nitrogen and the argon are separated. However, this is a very expensive process, due to major energy costs. Consequently, much research is carried out to develop membranes that more efficiently separate oxygen from air.

1.3 Motivation and scope of the present work:

Vapor-liquid equilibria (VLE) are very fundamental properties, which are always needed in order to design and operate separation processes. They form the basic criterion while choosing selective solvents for the absorption processes. Also, in order to do proper thermodynamic modeling, accurate equilibrium data for amine-water binary systems, measured over a wide range of temperature, pressure and concentrations are essential (Kim, 2009).

The present work is dedicated to measuring VLE data for two types (DEEA & DIPEA) amine systems. For this purpose, a modified Świątosławski ebulliometer was used. Experimental activity coefficients were then fitted to NRTL, Wilson and UNIQUAC models.

2.0 Theoretical background

2.1 Thermodynamic framework for VLE:

A system is said to be in equilibrium if only reversible process can take place in it. For homogenous phase at equilibrium, the intensive properties are same everywhere. Intensive properties are those which are independent of mass, size and shape of the phase; we are usually concerned about properties like temperature, pressure, composition (often expressed as mole fraction) etc (Prausnitz et al. 1999). The equilibrium criterion states that:

$$dT=0, \quad dP=0 \quad dG=0 \quad (2.1)$$

Where T is the absolute temperature, P the pressure and G the free enthalpy of system and it means that when a system is at equilibrium there is no change in its temperature, pressure or free enthalpy.

Phase equilibrium dictates how the molecular species get distributed in the liquid and vapor phases. The simplest way to define equilibrium condition for phase equilibria is by defining the Gibb's free energy G , which is the maximum amount of non expansion work that can be extracted from a closed system.

$$G = U - TS - (-PV) = H - TS \quad (2.2)$$

Where U is internal energy with the units of J; P is the pressure, Pa; V is the volume, m^3 ; T is temperature, K; S is entropy, JK^{-1} and H is enthalpy, J.

For a mixture, the total derivative of G is the sum of its partial derivatives with respect to temperature, pressure and composition and thus can be written as:

$$dG = \left(\frac{\partial G}{\partial T} \right)_{p, n_i} dT + \left(\frac{\partial G}{\partial P} \right)_{T, n_i} dP + \left(\frac{\partial G}{\partial n_1} \right)_{p, T, n_j} dn_1 + \left(\frac{\partial G}{\partial n_2} \right)_{p, T, n_j} dn_2 \dots \quad (2.3)$$

Where n_i is the number of moles of all components while n_j is the number of moles of all except the one which is being differentiated. At constant temperature and pressure the equation gets the form of:

$$dG_{p, T} = \mu_1 dn_1 + \mu_2 dn_2 \dots \dots \quad Or \quad (2.4)$$

$$dG_{P,T} = \left(\sum \mu_i dn_i \right)_{P,T} \quad (2.5)$$

For equilibrium at constant temperature and pressure the Gibb's energy is at its minimum (Prausnitz et al., 1999) which means

$$dG_{P,T} = 0 \quad (2.6)$$

For two phases in equilibrium, equation 2.6 yields:

$$dG_{P,T} = \sum_i \mu_i^V dn_i^V + \sum_i \mu_i^L dn_i^L = 0 \quad (2.7)$$

Where, V and L stand for vapor and liquid phases respectively. For a closed system where no chemical reaction is taking place $dn_i^V = -dn_i^L$ which goes on to show that at equilibrium (Prausnitz et al., 1999):

$$\begin{aligned} \mu_i^V &= \mu_i^L \\ T^V &= T^L \\ P^V &= P^L \end{aligned} \quad (2.8)$$

2.1.1 Fugacity and activity:

The chemical potential does not have an immediate equivalent in the physical world so there has to be some other auxiliary functions which can be used to define it in physical sense as well. One such useful auxiliary function is obtained by defining the concept of fugacity. The fugacity of component i in a mixture is defined as:

$$RTd \ln f_i = d\mu_i \quad \text{at constant temperature} \quad (2.9)$$

Where μ_i is the chemical potential of component i in the mixture while f_i is its fugacity. For a pure, ideal gas, fugacity is equal to the pressure while for a component i in a mixture of ideal gases it is equal to its partial pressure $y_i P$. Since all systems behave ideally at very low pressures so the definition of fugacity is completed by the limit (Prausnitz et al. 1999):

$$\frac{f_i}{y_i P} \rightarrow 1 \quad \text{as } P \rightarrow 0 \quad (2.10)$$

Lewis called the ratio of f/f° the activity, designated by the symbol a . The activity of a substance gives an indication of how 'active' a substance is relative to its standard state because it provides a measure of difference between the substance's chemical potential at the state of interest and that at its standard state. The temperature of the standard state must be the same as that of the state of interest (Prausnitz et al. 1999).

The fugacity provides a convenient transformation of the fundamental equation of phase equilibrium, eq. 2.8. By integrating eq. 2.9 with respect to composition at fixed T from a state of pure i to a mixed state, we get:

$$\mu_i^V - \mu_i^o = RT \ln \frac{f_i^V}{f_i^o} \quad (2.11)$$

Where μ_i^o and f_i^o are chemical potential and fugacity respectively for the pure fluid at the same temperature. When compared with a similar equation of liquid phase we get the expression:

$$\mu_i^V - \mu_i^L = RT \ln \frac{f_i^V}{f_i^L} = 0 \quad (2.12)$$

When we suppose that the standard state for both phases is the same, the standard of equilibrium can be written in terms of fugacity:

$$f_i^V = f_i^L \quad (2.13)$$

Eq. 2.13 states that the equilibrium condition in terms of chemical potentials can be maintained with its full significance even if the chemical potentials are replaced by fugacities.

The ratio of fugacity to the real gas pressure is called fugacity coefficient ϕ :

$$\frac{f_i}{y_i P_i} = \phi_i \quad (2.14)$$

The fugacity coefficient is the measure of non ideality of the system. It is just another way of characterizing the Gibb's excess functions at fixed temperature and pressure. For a mixture of ideal gases is $\phi_i=1$.

2.1.2 Activity and activity coefficient:

The activity of a substance, as defined above, can be written as:

$$a_i = \frac{f_i}{f_i^o} \quad (2.15)$$

While activity coefficients can be defined as:

$$\gamma_i = \frac{f_i}{x_i f_i^o} \quad (2.16)$$

Experimental activity coefficients of any specie i in the liquid can be calculated by measurable parameters as follows (Van Ness, 1995):

$$\gamma_i = \frac{y_i P}{x_i P_i^o} \cdot \Phi_i \quad (2.17)$$

Where

$$\Phi_i = \frac{\hat{\Phi}_i}{\Phi_i^o} \exp \left[\frac{-v_i^L (P - P_i^o)}{RT} \right] \quad (2.18)$$

At low to moderate pressures, the factor Φ_i has relatively less importance and can be neglected. The fugacity coefficients' ratio accounts for vapor phase non idealities while the exponent is often called *Poynting correction* and takes into account that the liquid is at a pressure P which is different from P_i^o . ' v ' is the molar volume at the system temperature and saturation pressure.

2.1.3 Standard and reference state:

The *reference state* is a state for a pure substance at specified temperature, pressure and the type of phase (S, L or V). The reference state is invariant to the system (P & T) throughout an entire thermodynamic problem (Kim, 2009).

Standard state is a state for a pure substance at a specified (T, P) and type of phase (S, L or V). The standard state T is always the same as the T of interest for the given calculation while the standard state P can be either a fixed P or the pressure of the system itself (Kim, 2009). The most common types of reference states are the pure component reference state (Raoult's law) and the indefinite dilution reference state (Henry's law) as stated below.

2.1.4 Normalization of the activity coefficients:

It is convenient to define activity in such a way that, for an ideal solution, it becomes equal to the component's mole fraction or, equivalently, the activity coefficient is equal to unity. Since we have distinguished between two types of ideality (Raoult's law & Henry's law), it follows that activity coefficients can be normalized in two different ways.

If activity coefficients are defined with reference to an ideal solution in the sense of Raoult's law, then for each component i , the normalization is:

$$\gamma_i \rightarrow 1 \text{ as } x_i \rightarrow 0 \quad (2.19)$$

Because this normalization holds for both solute and solvent, the above equation is called the *symmetric* conversion for normalization.

However, if activity coefficients are defined with reference to an ideal dilute solution, then the normalization becomes:

$$\begin{aligned} \gamma_1 \rightarrow 1 \text{ as } x_1 \rightarrow 0 & \quad (\text{Solvent}) \\ \gamma_2 \rightarrow 1 \text{ as } x_2 \rightarrow 0 & \quad (\text{Solute}) \end{aligned} \quad (2.20)$$

Because solute and solvent are not normalized in the same way so the above equation gives the *unsymmetric* convention for normalization.

2.1.5 Excess functions:

The thermodynamic properties of real solutions are expressed in terms of the excess functions, X^E . These excess functions give the difference between the observed thermodynamic functions and those of an ideal solution at the same conditions of temperature, pressure and composition. For phase equilibrium, the most useful excess property is the excess molar Gibb's energy. This is so because G^E can be directly related to the activity coefficient:

$$RT \ln \gamma_i = \left(\frac{\partial G^E}{\partial n_i} \right)_{T,P,n_j(j \neq i)} \quad (2.21)$$

Excess enthalpy H^E is also an important thermodynamic function which gives the isothermal enthalpy change per mole of solution when mixing two pure liquids without any chemical reaction. H^E data is very useful when it comes to modeling because it is directly related to the temperature dependency of the G^E thus resulting in *Gibb's Helmholtz equation*, which relates the change of G^E with temperature to H^E as (Kim, 2009):

$$\left[\frac{\partial(G^E / T)}{\partial T} \right]_{p,x} = -\frac{H^E}{T^2} \quad (2.22)$$

2.1.6 The Gibbs-Duhem equation:

The partial molar properties of different components in a mixture are related to one another by Gibbs-Duhem equation. The equation states that at constant temperature and pressure:

$$\sum_i x_i dm_i = 0 \quad (2.23)$$

Where m_i is any partial molar property. The equation hold for both real and ideal solutions and can be rewritten in terms of excess properties as:

$$\sum_i x_i dm_i^E = 0 \quad (2.24)$$

The equation can be used to calculate additional properties in the absence of some of the experimental data. For example the vapor phase composition may be calculated from the available P,T & x data. But in case we already have complete data, the equation can then be used to calculate the thermodynamic consistency of the available data. If the data satisfies Gibbs-Duhem equation, it is thermodynamically consistent and can be relied with but if the equation is not satisfied it is a possibility that the data is not reliable enough. Equation 2.24 can be written in terms of activity coefficients as:

$$\sum_i x_i d \ln \gamma_i = 0 \text{ at constant T,P} \quad (2.25)$$

It is a differential relationship between the activity coefficients of all components in the solution. For a binary solution though, we can write it as:

$$x_1 \frac{d \ln \gamma_1}{dx_1} = x_2 \frac{d \ln \gamma_2}{dx_2} \quad (2.26)$$

2.1.7 Modeling of data

There are different equations, which are available to estimate the relationship between activity coefficients and mole fraction. The three equations used in the present work are: NRTL, Wilson and UNIQUAC. Experimental activity coefficients were calculated using equation 2.17 and were fitted using these three models.

The NRTL equation

NRTL (non random, two liquid) is based on the concept of local composition. The NRTL equation for the excess Gibbs energy is (Prausnitz, 1999):

$$\frac{G^E}{RT} = x_1 x_2 \left(\frac{\tau_{21} G_{21}}{x_1 + x_2 G_{21}} + \frac{\tau_{12} G_{12}}{x_2 + x_1 G_{12}} \right) \quad (2.27)$$

Where:

$$\tau_{12} = \frac{g_{12} - g_{22}}{RT} \quad \text{and} \quad \tau_{21} = \frac{g_{21} - g_{11}}{RT} \quad (2.28)$$

$$G_{12} = \exp(-\alpha_{12} \tau_{12}) \quad \text{and} \quad G_{21} = \exp(-\alpha_{12} \tau_{21}) \quad (2.29)$$

g_{ij} is an energy parameter characteristic for the i - j interaction. Parameter α_{12} is related to the non randomness in the mixture. When α_{12} is zero, the mixture is completely random.

From equation 2.27 the activity coefficients are given as:

$$\ln \gamma_1 = x_2^2 \left(\tau_{21} \left(\frac{G_{21}}{x_1 + x_2 G_{21}} \right)^2 + \frac{\tau_{12} G_{12}}{(x_2 + x_1 G_{12})^2} \right) \quad (2.30)$$

$$\ln \gamma_2 = x_1^2 \left(\tau_{12} \left(\frac{G_{12}}{x_2 + x_1 G_{12}} \right)^2 + \frac{\tau_{21} G_{21}}{(x_1 + x_2 G_{21})^2} \right) \quad (2.31)$$

Wilson's equation:

Based on molecular considerations, Wilson took G^E to be a logarithmic function of liquid composition and proposed the following expression for excess Gibbs energy of a binary solution (Prausnitz, 1999):

$$\frac{G^E}{RT} = -x_1 \ln(x_1 + \Lambda_{12}x_2) - x_2 \ln(x_2 + \Lambda_{21}x_1) \quad (2.32)$$

The activity coefficients derived from this equation are given as:

$$\ln \gamma_1 = -\ln(x_1 + \Lambda_{12}x_2) + x_2 \left[\frac{\Lambda_{12}}{x_1 + \Lambda_{12}x_2} - \frac{\Lambda_{21}}{x_2 + \Lambda_{21}x_1} \right] \quad (2.33)$$

$$\ln \gamma_2 = -\ln(x_2 + \Lambda_{21}x_1) + x_1 \left[\frac{\Lambda_{12}}{x_1 + \Lambda_{12}x_2} - \frac{\Lambda_{21}}{x_2 + \Lambda_{21}x_1} \right] \quad (2.34)$$

The equations have two adjustable parameters Λ_{12} and Λ_{21} . They are given as:

$$\Lambda_{12} = \frac{v_2}{v_1} \exp\left(-\frac{\lambda_{12} - \lambda_{11}}{RT}\right) \quad (2.35)$$

$$\Lambda_{21} = \frac{v_1}{v_2} \exp\left(-\frac{\lambda_{21} - \lambda_{22}}{RT}\right) \quad (2.36)$$

Where v_i is the molar liquid volume of the pure component i and λ is the interaction energy between the molecules (Wilson, 1963).

UNIQUAC equation:

For a multicomponent system, the UNIQUAC equation for the molar excess Gibbs energy is given by the sum of (Abram & Prausnitz, 1975):

$$\frac{G^E(\text{combinatorial})}{RT} = \sum_i x_i \ln \frac{\Phi_i}{x_i} + \frac{z}{2} \sum_i q_i x_i \ln \frac{\theta_i}{\Phi_i} \quad (2.37)$$

And

$$\frac{G^E(\text{residual})}{RT} = -\sum_i q_i x_i \ln \left(\sum_j \theta_j \tau_{ji} \right) \quad (2.38)$$

Where

$$\Phi_i = \frac{r_i N_i}{\sum_j r_j N_j} = \frac{r_i x_i}{\sum_j r_j x_j} \quad \theta_i = \frac{q_i N_i}{\sum_{j=1}^m q_j N_j} = \frac{q_i x_i}{\sum_{j=1}^m q_j x_j} \quad (2.39)$$

And
$$\tau_{ji} = \exp\left(-\frac{u_{ji} - u_{ii}}{RT}\right) \quad (2.40)$$

The coordination number z is set equal to 10. For any component i , the activity coefficient is given by:

$$\ln \gamma_i = \ln \frac{\Phi_i}{x_i} + \frac{z}{2} q_i \ln \frac{\theta_i}{\Phi_i} + l_i - \frac{\Phi_i}{x_i} \sum_j x_j l_j - q_i \ln \left(\sum_j \theta_j \tau_{ji} \right) + q_i - q_i \sum_j \frac{\theta_j \tau_{ij}}{\sum_k \theta_k \tau_{kj}} \quad (2.41)$$

Where
$$l_j = \frac{z}{2} (r_j - q_j) - (r_j - 1)$$

2.1.8 Thermodynamic consistency of data:

Equilibrium data is always prone to some errors, the intensity of which depends upon the accuracy of measurements and the type of instrument used. As described before, large random errors can be detected by looking at the smoothness of the curves obtained e.g. in x-y diagrams but in some cases the smoothness of curve cannot be taken as a parameter for the reliability of data since experimental data can be subject to a systematic error which does not show up as scatter in the measured points (Kim, 2009).

According to phase rule, only P , T and x data is sufficient to characterize the system but if the composition of both phases is known then the extra information (y values) can be used to test the data for thermodynamic consistency. The Gibbs Duhem equation interrelates activity coefficients of all components in a mixture so if the data of all activity coefficients are available they should satisfy Gibbs Duhem equation, which if they do, can be taken as an indication of the data's consistency (Kim, 2009).

$$\frac{G^E}{RT} = x_1 \ln \gamma_1 + x_2 \ln \gamma_2$$

Since NRTL, Wilson and UNIQUAC equations are inherently thermodynamically consistent so the difference between the parameters predicted by models and those obtained from experiment gives an idea about the thermodynamic consistency of the experimental data.

2.2 Fourier Transform Infrared (FTIR) spectroscopy:

2.2.1 Introduction

FT-IR spectroscopy is a technique which can be used to obtain the molecular fingerprints of any unknown sample. In infrared spectroscopy, IR radiations are passed through the sample. Some of these radiations are absorbed by the samples while the rest of them are transmitted through. This

results in an absorption/transmission spectrum of the sample under consideration. Since different molecules have different absorption/transmission characteristics so we always obtain a unique infrared spectrum from a specified sample mixture.

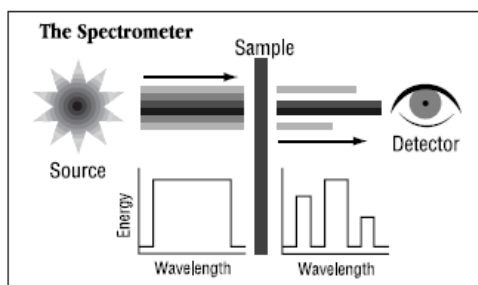


Figure 1.4: A simplified view of IR spectroscopy [Thermo Nicolet, 2001]

The figure presents a very basic working principle of spectroscopy. The radiations coming from the source fall on the sample. Some of these radiations get absorbed while some get transmitted through thus resulting in a change in the wavelength of incident radiations. The infrared spectrum thus obtained represents the fingerprint of the sample with absorption peaks which correspond to the frequencies of vibration between the atomic bonds present in the sample. Since every compound has a unique atomic configuration so this results in a characteristic spectrum for each compound. In this way quality of the sample can be identified very positively. Also the size of each peak gives an indication of the quantity of specie present in the sample. So the spectrum can be used to extract information both about the type and quantity of the species present in the sample at the same time. Also the quality and consistency of the sample can be tested using FT-IR spectroscopy. All these qualities make FT-IR spectroscopy a powerful and reliable tool for infrared spectroscopy.

2.2.2 Why FT-IR?

Older techniques used for infrared spectroscopy were of dispersive type which separated the incident infrared radiation into individual energy frequencies. The instruments used for this purpose can either be a prism or grating. The result of this dispersion is a spectrum showing intensity against frequency. The main limitation associated with dispersive techniques is the slow scanning process; also, it is desired to measure all infrared frequencies at the same time rather than measuring them individually. Using FT-IR can eliminate both these limitations as a new scan is collected every second and it accounts for all the frequencies simultaneously. Moreover it requires no external calibration so the measurements are always very precise.

2.2.3 How it works?

The main components of FT-IR spectrometer are the infrared source, interferometer, sample cell, detector and data processing unit. Interferometer is responsible for measuring all the infrared frequencies simultaneously. It uses a beamsplitter (half transparent mirror) to divide the incident infrared beam into two optical beams. One beam is reflected off a mirror which is fixed in its place while the other half is reflected off a mirror which is moving very small distance (few millimeters) away from the beamsplitter. When these two reflected beams are reunited at the

beamsplitter they produce interference. The strength of the interference is dictated by the optical path difference between the two beams and this path difference is caused by the position of the moving mirror.

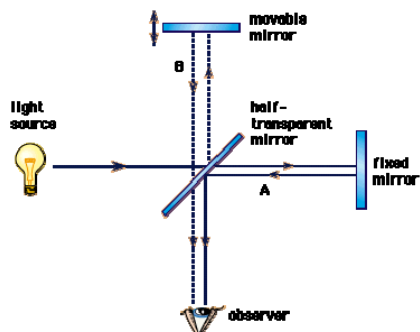


Figure 1.5: Working of Interferometer [2i]

The resulting signal is called interferogram and it has the unique quality that every data point (which is a function of the moving mirror) has information about every infrared frequency that is coming from the source.

The interferogram cannot be interpreted directly because the fundamental measurement obtained by FT-IR is in time domain. In order to get round this problem Fourier transform is used which converts the interferogram into a spectrum which is much easier to interpret.

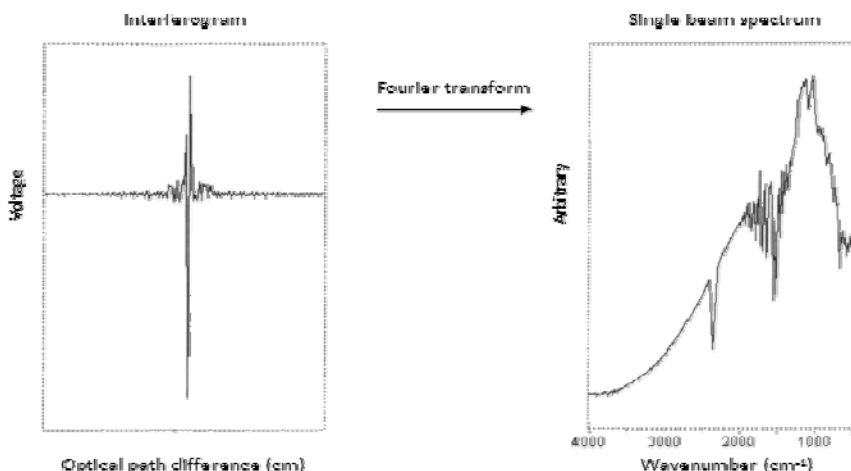


Figure 1.6: Fourier transformation of an interferogram to give spectrum [3i]

The infrared spectrum is obtained by passing a parallel, polychromatic light from an IR source through the interferometer from where it is directed onto the sample thus producing an interferogram. This interferogram then undergoes Fourier transformation thus producing an absorbance/transmittance spectrum.

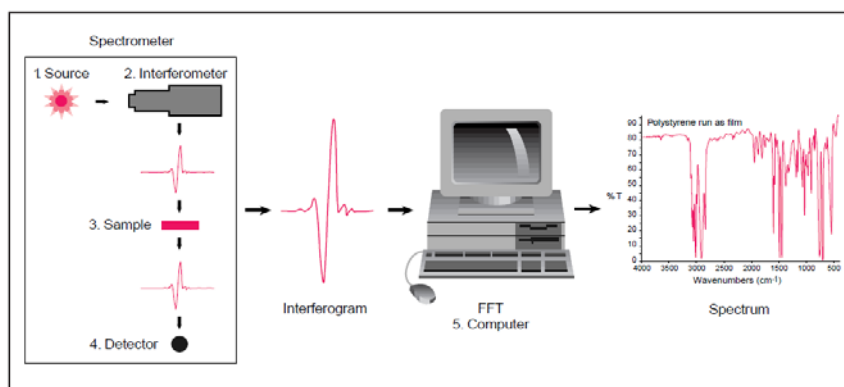


Figure 1.7: Steps in obtaining spectrum from FT-IR spectrometer [Thermo Nicolet, 2001]

But there needs to be a relative scale for the absorption intensity of all the samples. This relative scale is produced by measuring a background spectrum and subtracting it from the spectrum obtained for each sample. Usually air or distilled water spectrum is used as background.

2.2.4 Interpreting the FT-IR spectra:

The spectra obtained from FT-IR give simultaneous indication of both quantity and quality of the sample under consideration. Unique absorption band frequencies are associated with various chemical species which are used to identify them while the peaks in the spectrum give an indication of the quantity of compound present. Absorbance can be defined as the logarithm of the inverse transmittance.

$$\log (I_0/I) = \log (1/T)$$

According to Beer-Lamberts law; “there exists a linear relationship between the absorption and concentration of an absorber of electromagnetic radiation”.

$$A = a \cdot b \cdot c$$

Where

A= absorbance

a= wavelength dependent absorptivity coefficient

b= optical path length (distance the beam travels in sample)

c= concentration

As Beer-Lamberts law is additive in nature so the total absorbance A is the sum of the values of A of each gas component. This allows for simultaneous analysis of multiple compounds in the mixture. If the concentration range of the sample is not very broad a plot of concentration against

absorbance will give a straight line but as concentration range starts becoming broader, the change in sample environment can cause deviation from Beer-Lamberts law.

The spectral resolution defines the ease of differentiating between different wavelengths of radiation in the absorption spectrum while the number of scans gives an indication of signal to noise ratio. Adding more and more spectra gives a better signal to noise ratio (SNR). SNR is directly proportional to the square root of number of scans which means the higher the number of scans the lesser would be noise in the spectrum. (Aslak Einbu)

$$\text{SNR} \propto (\text{no. of scans})^{1/2}$$

For any type of analysis, optimum resolution and number of scans need to be established first by trying various combinations. Operating at higher resolution and higher number of scans means more time to obtain the spectrum. In the present work resolution of 4 cm^{-1} and the same (i.e. 4) number of scans were found to give good enough results.

2.2.5 FT-IR at NTNU; FLTA2000-104:

The FT-IR spectroscope available with NTNU/Sintef is FLTA200-104. It can operate in the spectral MIR (mid infrared) range of 6500-500. The resolution can be varied from 1 to 32 cm^{-1} . The software used to obtain spectra is called PAS (Protea analyzer software). Purging of system is done continuously using Purge gas generator which employs moisture and CO_2 free air to purge the system continuously.



Figure 1.8: ABB's FLTA2000 FT-IR spectroscope (*FLTA200 users' guide*)

“The accessory used for the analysis of liquid samples with FT-IR spectroscope is called Attenuated total reflection (ATR). The ATR operates by measuring the changes in the incident infrared beam which passes through the sample after being reflected internally by the crystal.

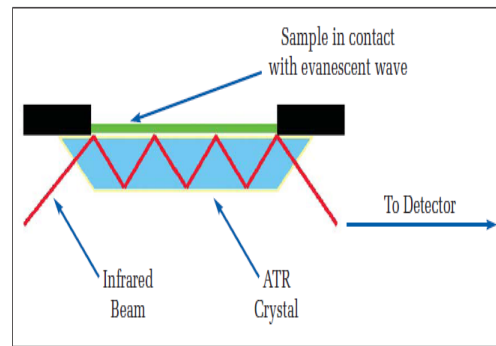


Figure 1.9: Pike miracle ATR and its operating principle (PerkinElmer)

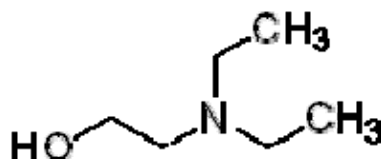
The beam is directed onto an optically dense crystal with high refractive index at a certain angle. The internal reflectance creates an evanescent wave which extends beyond the surface of the crystal into the sample held in contact with the crystal (Diamond in this particular case). The penetration into the sample is only a few microns (0.5-5 micron) beyond the crystal surface. In the regions of infrared spectrum where the sample absorbs energy the wave will be attenuated. The attenuated energy from each wave is passed back to the IR beam, which then exits the opposite end of the crystal and is passed to the detector in the IR spectrometer. The system then generates an infrared spectrum.” (PerkinElmer)

3.0 VLE measurements

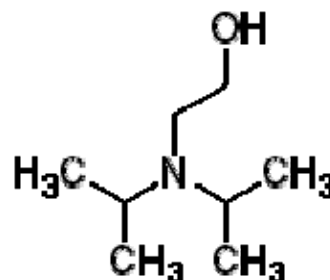
3.1 Overview of the present work:

During the course of present work VLE measurements of two types of binary systems were carried out, namely: DEEA-H₂O and DIPEA-H₂O system.

DEEA (2- Diethylaminoethanol) and DIPEA (2-Diisopropylaminoethanol) are both tertiary amines with the chemical formulas as:



DEEA



DIPEA

Amine name	MW (g/mol)	Purity (%)	Product of	Temp. tested
DEEA	117.19	>=99.5	Sigma Aldrich	50, 60, 80 & 95°C
DIPEA	145.24	99+%	Sigma Aldrich	60, 80 & 95°C

Table 3.1: Properties and testing temperature for amines used in this work

The VLE experiments were performed in the modified Świątosławski ebulliometer. The vapor and liquid samples were collected which were then analyzed for amine quantification. All this data was then used to calculate experimental activity coefficients, which were subsequently fitted to NRTL Wilson and UNIQUAC models.

3.2 Experimental techniques:

There are two ways of determining the temperature dependence of saturated vapors' pressure, namely: Dynamic and Static methods. In the dynamic method pressure is kept constant and temperature is measured when liquid and vapor phases are in equilibrium. While in the static method temperature is kept constant and pressure is measured at equilibrium.

Ebulliometry is form of dynamic method which was introduced by Cottrell and Washburn in 1919. Świątosławski and his school took the credit for perfecting the technique for very precise measurements of boiling points of liquids. An ebulliometer is based on the principle of the Cottrell pump, a kind of narrow vertical tube extending to the bottom of test tube where it ends

in a funnel. When the liquid is heated, vapors rise through the tube while carrying slugs of liquid with them. The boiling liquid, lifted through this tube, flows on a horizontal plate from where it is led to the thermometer which is placed in the vapor space (Hála et al.1958). Although the technique is very effective one but it cannot be used as effectively when measuring the boiling point of a homogenous mixture with large boiling point difference. For this purpose Świątosławski made some modifications to the existing apparatus which is also used in the present work. It allows sampling of liquid phase and vapor condensed phase and the circulation is maintained continuously by Cottrell pump.

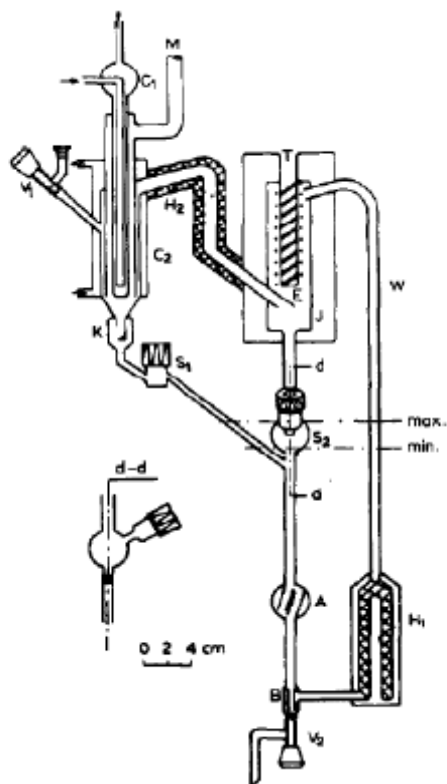


Figure 3.1: The ebulliometer used in the present work. Where H₁, Cottrell pump; A,B, Mixing devices; K, drop counter; C₁,C₂, Condensers; E, equilibrium chamber; T, thermowell, V₁, valve for introducing samples; V₂, valve for removing liquid; H₂, Heater for prevention of vapor condensation; S₁, Vapor condensate sampling; S₂, Liquid sampling.

Meanwhile the static method is a lot simpler in which the solution is charged into a closed n evacuated cylinder and it is place in a thermostat. The filled cylinder is rotated and shaken until equilibrium is established. Once the equilibrium has been established samples from liquid and vapor phases are collected.

3.3 Experimental procedure:

The ebulliometer can operate either in isothermal or isobaric mode. While operating in the isothermal mode, pressure is adjusted until the desired temperature is achieved but when

operating in isobaric mode temperature is adjusted until the point of constant desired pressure. The data obtained in this work is all from isothermal experiments.

The equilibrium still is made of glass and has a volume of 200 ml. The maximum conditions under which the apparatus can be operated are 200°C and 1 bar. Temperature is measured with a calibrated Pt-100 resistance thermocouple which has an uncertainty of $\pm 0.05\text{K}$ while pressure is measured and controlled by a calibrated DPI520 with an uncertainty range of $\pm 0.3\text{ Kpa}$.

The ebulliometer was purged with N_2 before starting the experiment. For each run $\sim 80\text{ ml}$ of solution was charged and the pressure was reduced down to the lowest possible values to remove any air present in the system. Afterwards, the pressure was set at the desired value and heating of solution was started by electrical heaters. Once boiling got started the pressure was adjusted to keep the temperature as close as possible to the desired value. Samples from liquid and vapor condensate phase were collected after no change was observed in temperature or pressure for at least 10 minutes.

3.4 Analyses of liquid & vapor phase samples:

The liquid and vapor phase samples were collected by using disposable plastic syringes and were placed in sealed vials of $\sim 5\text{ ml}$ and $\sim 2\text{ ml}$ volume respectively. Amine analyses of the binary liquid phase samples were carried out by titration. Samples with higher concentration of amine were titrated against $0.1\text{ M H}_2\text{SO}_4$ while the low concentration samples were titrated against $0.01\text{ M H}_2\text{SO}_4$. The vapor phase samples could not be analyzed by titration because of their very small size ($\sim 1\text{ ml}$ each). Although in the prior related works the vapor phase samples had been analyzed either by LC-MS or GC but for the present work it was decided to use FTIR spectroscopy for the said purpose. Since FTIR has not been used very extensively for amine analyses so a lot of effort and time was dedicated to understanding and implementing the technique on the present work.

3.5 Results and discussion:

3.5.1 FTIR results:

Since FTIR analyses made an important part of the present work so it is appropriate to discuss this technique (and the results obtained by it) in detail before going further to discuss the vapor liquid equilibrium data.

The basics of FTIR spectroscopy has been discussed in detail in the preceding chapter. As discussed earlier, the vapor phase samples from the ebulliometer were to be tested by using the FTIR technique. The spectra of all samples were produced using FTIR and the results were then imported to The Unscrambler (which is a ‘multivariate data analyses’ software) in ‘Grams’ format. Calibration model was prepared based on the spectra obtained from calibration solutions and based on this model the quantities of DEEA in the experimental samples were predicted.

In order to verify the results obtained by FTIR (especially in the low concentration range) some vapor phase samples were sent to Sintef where they were tested using LCMS technique (Table 3.3). Moreover, all the liquid phase samples were also tested by FTIR and the results thus obtained were compared with the titration results (Table and Figure 3.2).

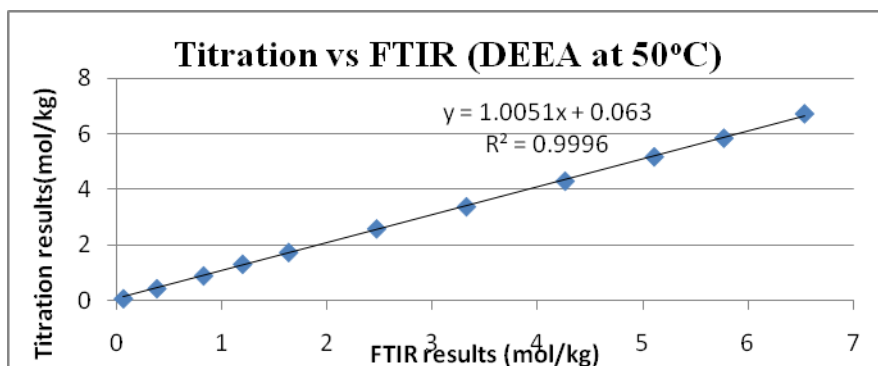
Sample	Predicted	Titration	Diff	Sample	Predicted	Titration	Diff
	mol/kg	mol/kg	%		mol/kg	mol/kg	%
				DEEA_953	6.557	6.684	1.89
AIR_D602	0.415	0.433	4.22	DEEA_954	6.160	6.172	0.19
AIR_D603	0.871	0.888	1.95	DEEA_955	5.850	5.942	1.55
AIR_D604	1.585	1.688	6.10	DEEA_956	5.046	5.058	0.23
AIR_D605	2.440	2.496	2.24	DEEA_957	4.211	4.265	1.27
AIR_D606	3.299	3.368	2.05	DEEA_958	0.868	0.913	4.97
AIR_D607	4.159	4.173	0.34	DEEA_959	1.715	1.759	2.50
AIR_D609	6.518	6.663	2.17	DEEA_9510	2.533	2.572	1.52
AIR_D610	5.820	5.905	1.43	DEEA_9511	3.476	3.463	-0.38
AIR_D611	5.021	5.032	0.21				
D_11	0.300	0.295	-1.56	DEEA_502	0.381	0.4398	13.37
D_12	0.680	0.732	7.08	DEEA_503	0.825	0.898	8.13
D_13	1.386	1.387	0.07	DEEA_504	1.196	1.316	9.12
D_14	2.037	2.136	4.61	DEEA_505	1.634	1.7385	6.01
D_15	2.699	2.759	2.16	DEEA_506	2.471	2.585	4.41
D_16	3.534	3.506	-0.81	DEEA_507	3.325	3.376	1.51
D_802	6.340	6.459	1.83	DEEA_509	6.541	6.712	2.54
D_803	5.572	5.624	0.92	DEEA_510	5.774	5.836	1.05
D_804	4.955	4.936	-0.38	DEEA_511	5.112	5.164	1.01
D_805	4.107	4.096	-0.27	DEEA_512	4.264	4.295	0.72

Table 3.2: Liquid phase comparative results of FTIR and Titration

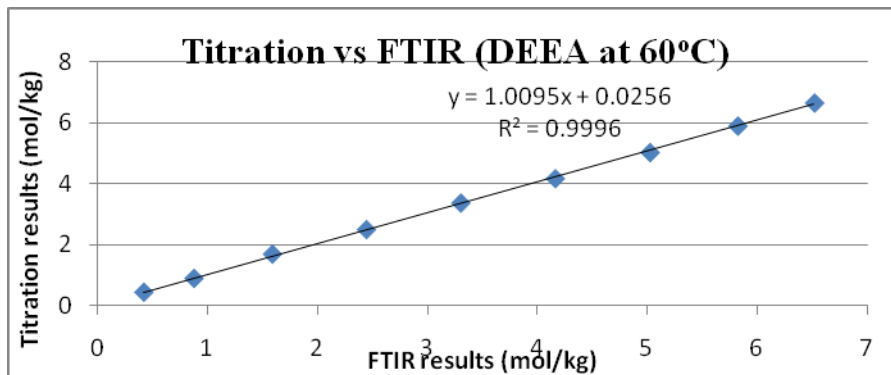
3.5.1.1 Discussion on the FTIR results:

Comparing the two results (Table 3.2) show that most of them are quite close to each other (with the difference being less than 2% in most cases). This is especially true if we don't take the 50°C samples into account, which due to some unknown reason show unusually bigger differences. Also the 50°C samples have relatively larger deviations when it comes to The Unscrambler results (see appendix 1) Although the difference between the two analyses' results is quite random but one obvious trend which can be extracted from these results is that the difference becomes increasingly large with decreasing amine concentration. There were different models developed in The Unscrambler to predict the amine concentrations and one thing which came out of these different models is that the predictions becomes more and more precise and accurate as the number of calibration samples increase in the interested concentration range. If less number

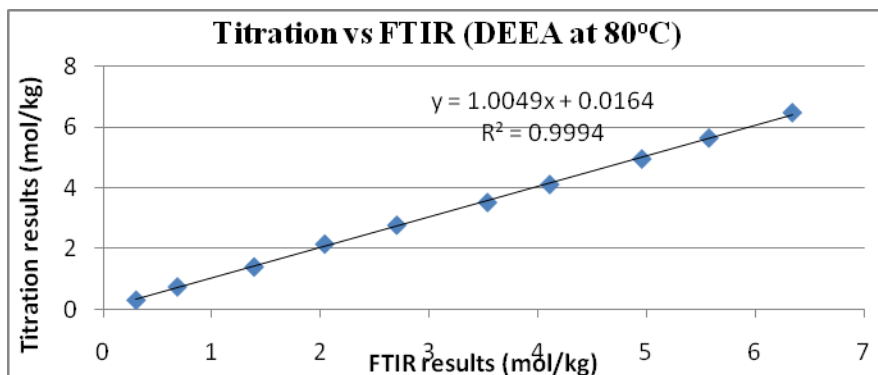
of calibration solutions is used the prediction results show large deviations which render the results less reliable. Although the results shown above are based on the predictions made by the



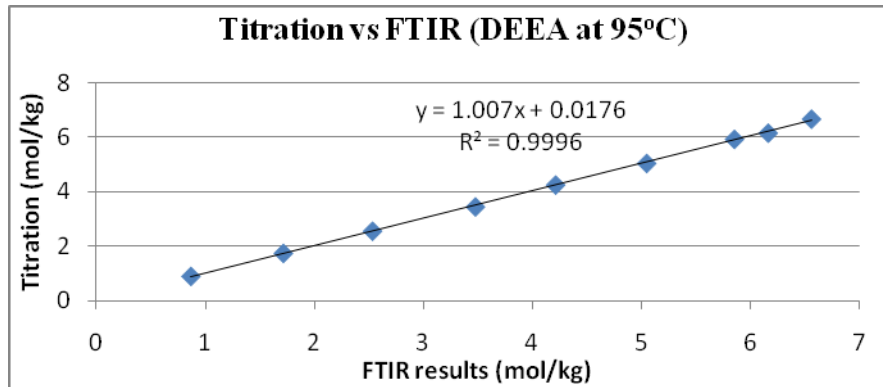
(a)



(b)



(c)



(d)

Figure 3.2 (a, b, c, d): Plots for comparison of FTIR and titration results

best possible model but it was later realized that may be an even higher number of calibration solutions especially in the lower concentration range may have further improved the results. But one thing which can be concluded with great certainty is the fact that the more closely ranged the calibration solutions are the better the results get. Figure 3.2 shows the plots produced from the data given in Table 3.2 thus providing graphical evidence of the similarity of these results.

As described earlier, some of the low (amine) concentration vapor phase samples were also sent for LCMS analyses and results were again compared with the ones obtained from FTIR.

Sample	LCMS	FTIR	Diff	Liquid phase amine
	mo/kg	mol/kg	%	Wt %
D11	0.609	0.626	2.68	3.58
D12	1.18	1.24	4.32	9.053
D502	0.413	0.498	16.91	5.797
D503	0.673	0.785	14.14	11.55
D602	0.531	0.586	9.31	5.56
D603	0.900	0.945	4.731	11.35
D957	1.72	1.718	-0.570	12.87

Table 3.3: Comparative results of LCMS and FTIR

Here again it can be seen that the difference between the two values is quite random but the problem here is that the LCMS results cannot be trusted with 100% certainty either. This is because, due to a mistake, only one sample was sent to Sintef for analyses instead of the usual two (sample A & B) so the repeatability of these LCMS results cannot be verified either. All the

above samples are from vapor phase but the last column shows the corresponding liquid phase concentration to give an idea about the overall concentration of the system under consideration.

The analyses of these results then bring us to the discussion of deciding as to which of these is a better technique when it comes to the measurement of very low concentration samples? Although titration and FTIR are two totally different analyses techniques with the former being a time tested and proven one but when it comes to judging FTIR, just by looking at the spectra obtained from it one can say with great certainty that the results obtained from it should be as trustworthy and repeatable as titration, if not more. This theory gets its backing from the fact that amine concentrations as small as 1% (liquid phase) show up in the spectra quite clearly (Figure 3.3). Once you have certain specie detected in the spectra, the rest should then depend only on the calibration model and the predictions made by it and as discussed above if the calibration model is based on sufficient number of closely ranged solutions then the results are very precise and repeatable.

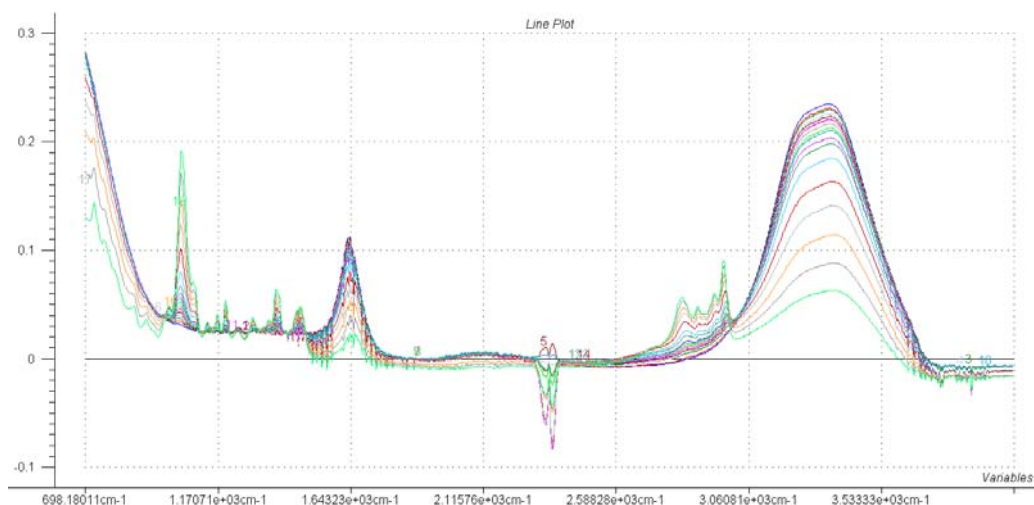


Figure 3.3: Calibration solutions' spectra

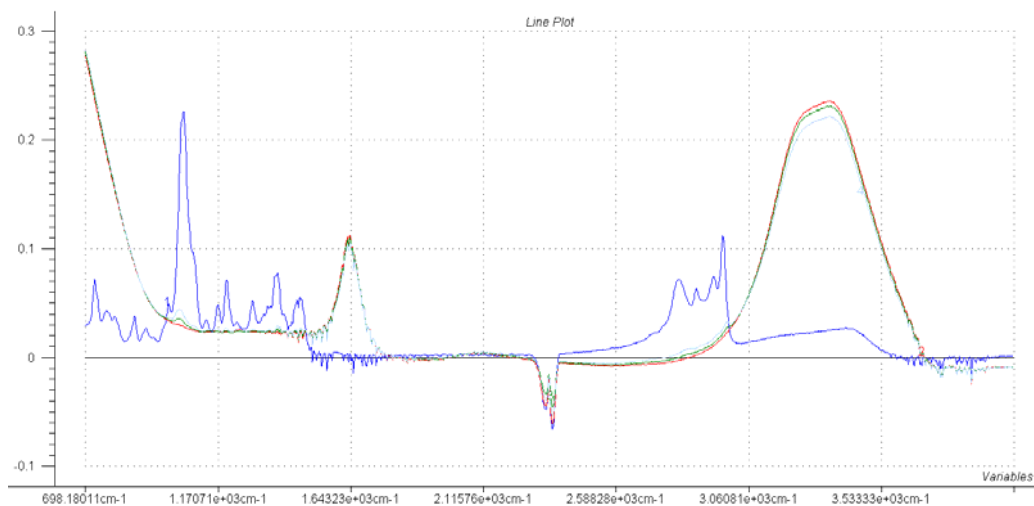
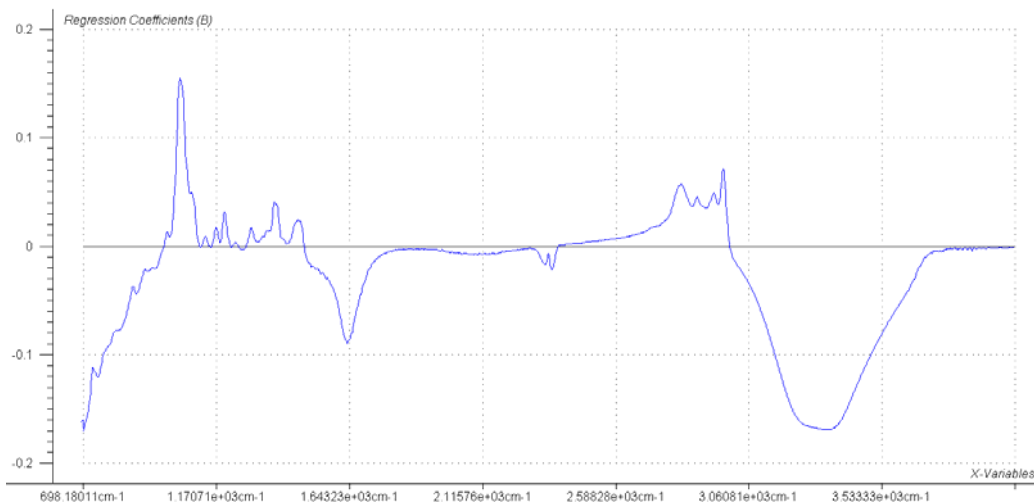
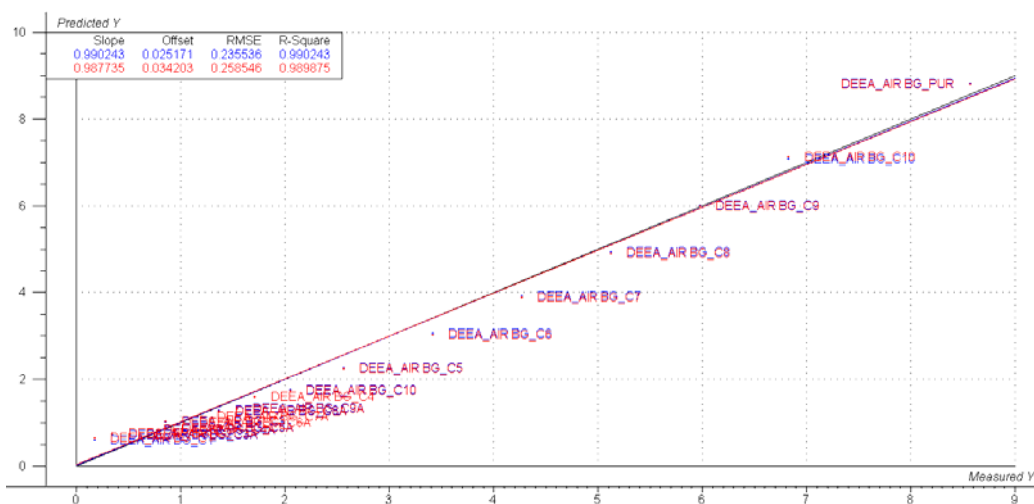


Figure 3.4: Blue, Pure DEEA, Red, 0.96 wt%, Green, 5.56 wt %, Light blue, 11.35 wt%



(a)



(b)

Figure 3.4.1: Regression results from The Unscrambler (a) The selected spectra (b) Prediction vs. measured plot

It can be seen from the spectral plot (Fig 3.3) that DEEA shows quite a few small and large peaks in the region $700\text{-}1500\text{ cm}^{-1}$ but the biggest of these lie in the wavelength range of $1000\text{-}1110\text{ cm}^{-1}$. The spectra have been obtained with air background and while predicting the concentration of unknown samples, the whole spectra were used because of the fact that DEEA shows so many peaks in the entire wavelength range so it was observed that full spectra gives better results. Figure 3.4.1 shows the regression results obtained in The Unscrambler for liquid phase samples. Figure 3.4.1(a) shows a regression coefficient plot which can be used to see the entire range of wavelengths (for all samples under consideration) and can be also used to select specific regions/peaks for model improvement. While Fig 3.4.2 is a ‘predicted vs. measured’ plot, which gives information about the quality of the model itself.

3.6 Vapor pressure data of pure Water:

First of all Water was tested in the Ebulliometer in order to get accustomed to the operation of apparatus and also to validate the precision and accuracy of the results. The experimental data is compared with the Riedel correlation in figure 3.5. The parameters for the correlation were taken from Perry's chemical engineers' handbook (8th edition).

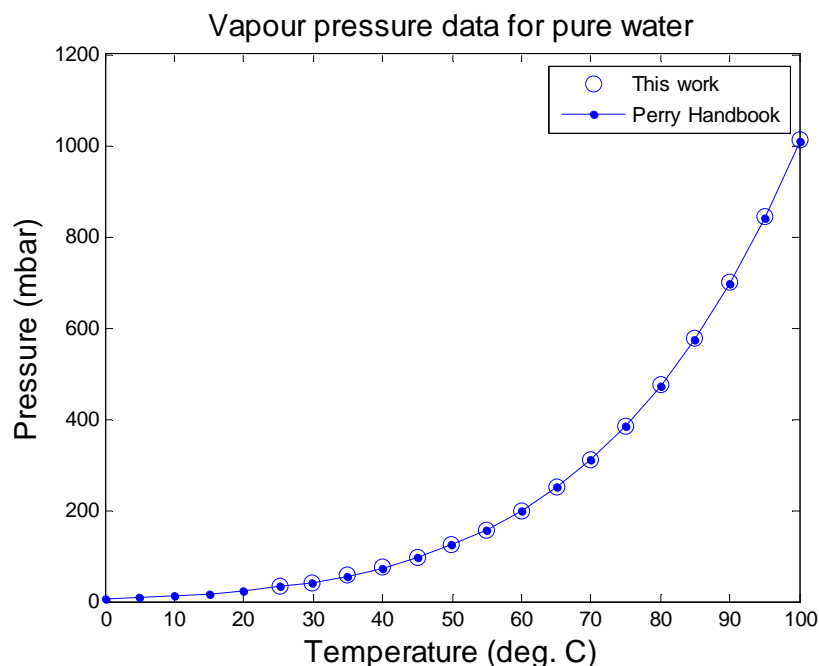


Figure 3.5: Water vapor pressure data from experiment and Riedel correlation

As it can be seen from the figure the experimental data is in perfect agreement with the correlation values, which speaks for the precision of the apparatus.

3.7 Vapor pressure data for pure DEEA and DIPEA:

The vapor pressure of pure DEEA and DIPEA were measured up to a total pressure of 1 bar. Since amines usually have high boiling points so the presence of even a very small amount of water in the system can result in increased total pressure especially at higher temperatures. The design of ebulliometer is such that it is very difficult to remove all the water from the system in one go. For this purpose the ebulliometer was first flushed with nitrogen and pure amine for 2-3 times and then fresh amine was boiled and discharged for as many time as required to be certain of no water contents in the system. With DEEA it took just three boils but with DIPEA it took around 5 boils before the system became totally free of water (Complete data in appendix 3).

The experimental data was then fitted to Antoine and Riedel equations (Figure 3.6). Note that the DIPEA data was fitted only to Antoine equation). The Antoine equation looks to give a better fit than Riedel in the case of DEEA. The vapor pressure data of pure DEEA was also compared with the one obtained from DOW chemical and it gives a fairly good fit. The very small difference between the data obtained in the present work and that of DOW chem. can be attributed to the quality and purity of the chemical used because DEEA used in this work was the

product of Sigma Aldrich, not of DOW chem. The second possible reason for this difference can be the presence of very small amount of water in the system as even negligible quantities of water can cause an increase in the vapor pressure. Although all efforts were made during the work to expel water from the system but still this possibility cannot be totally ruled out.

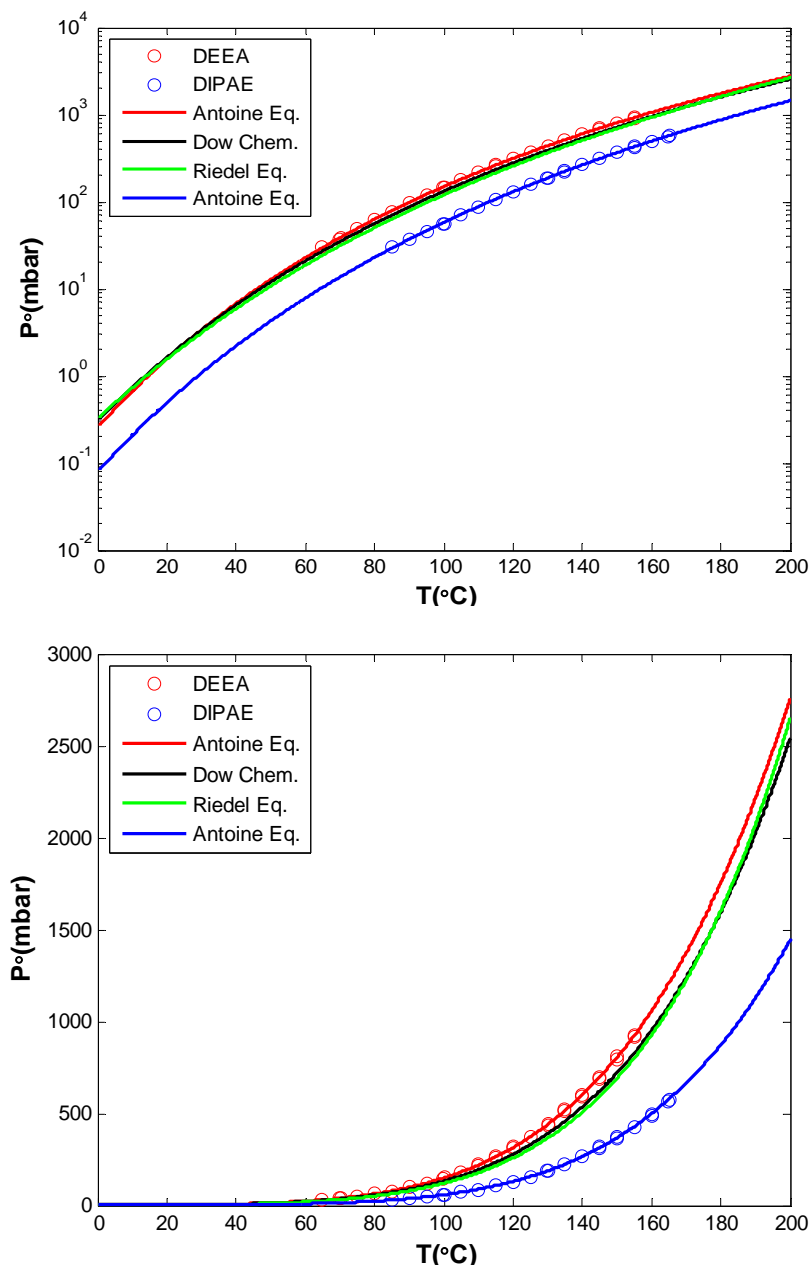


Figure 3.6: Vapor pressure data for pure DIPEA and DEEA

Antoine equations for DEEA and DIPEA are given below.

$$\text{DEEA:} \quad \ln(P^\circ / \text{mbar}) = A + \frac{B}{(T / ^\circ C) + C}$$

$$A = 15.7839 \pm 0.2$$

Where $B = -2903.8346 \pm 86$

$$C = 169.29091 \pm 4$$

$$\text{DIPEA:} \quad \ln(P^\circ / \text{mbar}) = A + \frac{B}{(T / ^\circ C) + C}$$

$$A = 16.6404 \pm 0.4$$

Where $B = -3660.57024 \pm 230$

$$C = 190.8672 \pm 10$$

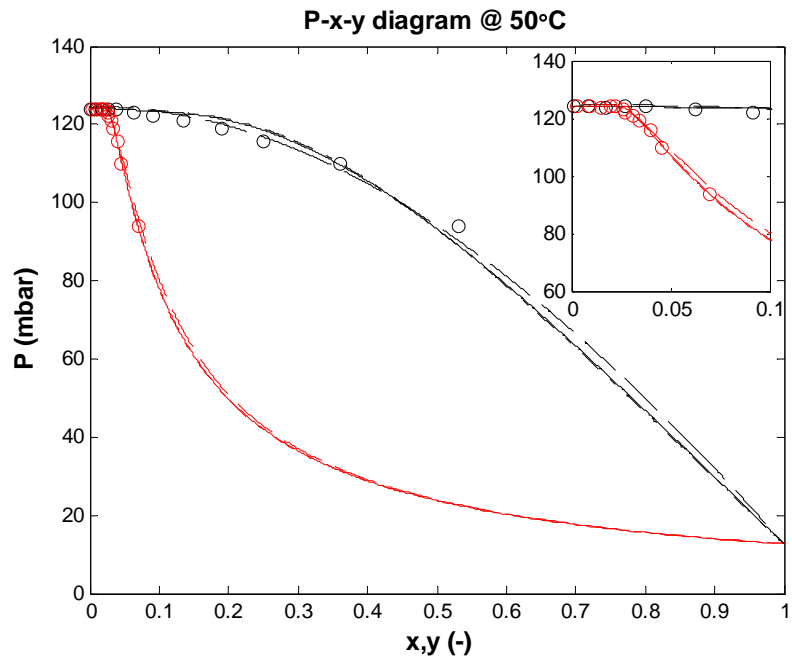
3.8 VLE of DEEA-H₂O solution:

VLE data for DEEA was measured at 50, 60, 80 and 95°C for varying concentration. Experimental data thus obtained was used to calculate experimental activity coefficients which were then fitted to NRTL, Wilson and UNIQUAC models. The results are presented in x-y, P-x-y and γ -x plots below.

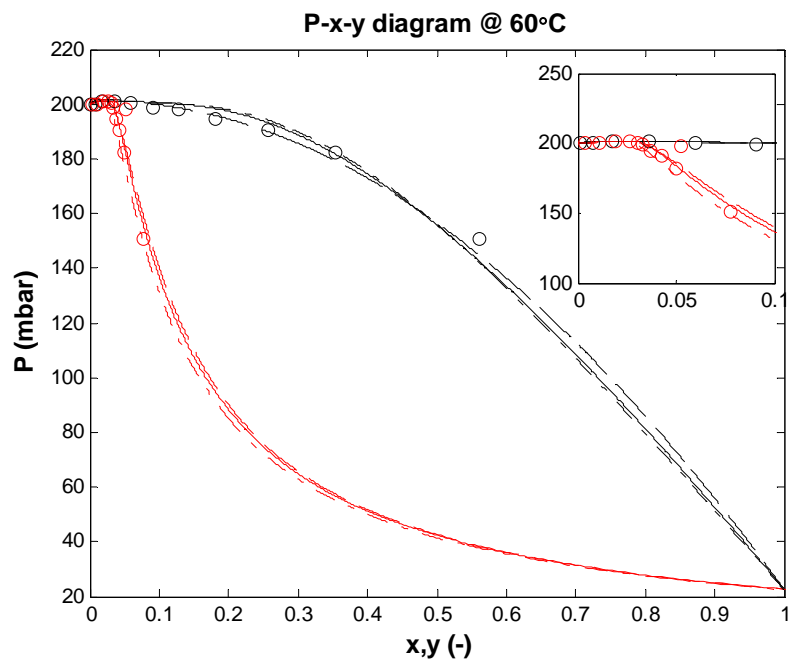
X-y diagrams can be a very good indication of the accuracy of the results and can be used as a first tool to detect any random error in the data. Coming back to the present work, vapor phase concentrations of DEEA were plotted against the liquid phase concentrations (Fig. 3.6) at different temperatures. It can be seen from these plots that at very low concentrations the x values are almost equal to those of y values which goes on to state that at these concentrations an azeotrope is formed between the two. The occurrence of these *azeotropic points* is of great significance, especially in distillation since it is not possible to separate the given mixture into its pure constituents under these conditions (Hála et al. 1958). As stated earlier, the liquid phase samples were analyzed for amine by titration while FTIR spectroscopy in combination with The Unscrambler was used to predict the vapor phase concentration and the consistency obtained in these diagrams in terms of vapor phase concentration gives an idea about the performance of FTIR itself.

The P vs. x-y plots (Figure 3.7) give an idea about the isothermal dependence of total pressure on liquid and vapor phase compositions. The lower concentration region again shows the tendency of azeotrope formation. Since at azeotropic points $y_i = x_i$ so

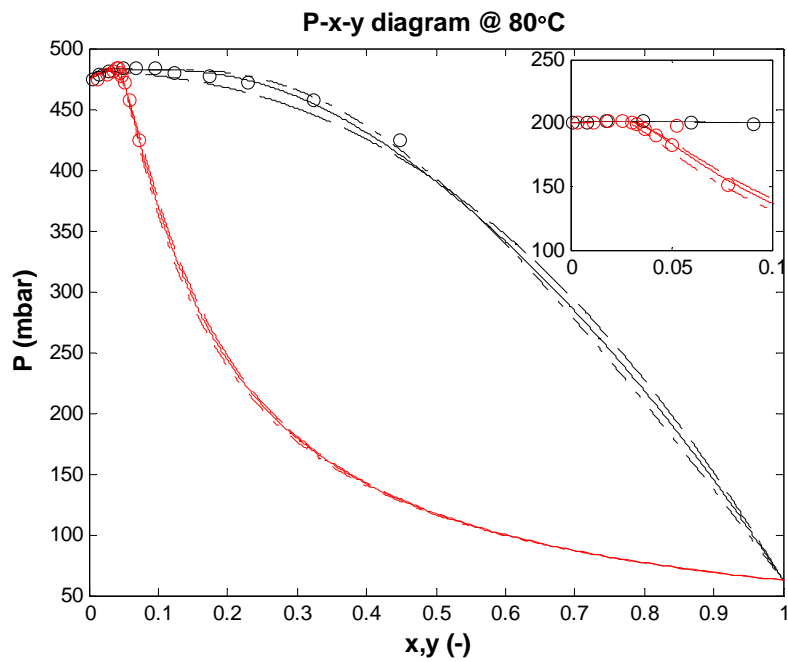
$$\gamma_1 = P/P^\circ_1 \quad \text{and} \quad \gamma_2 = P/P^\circ_2$$



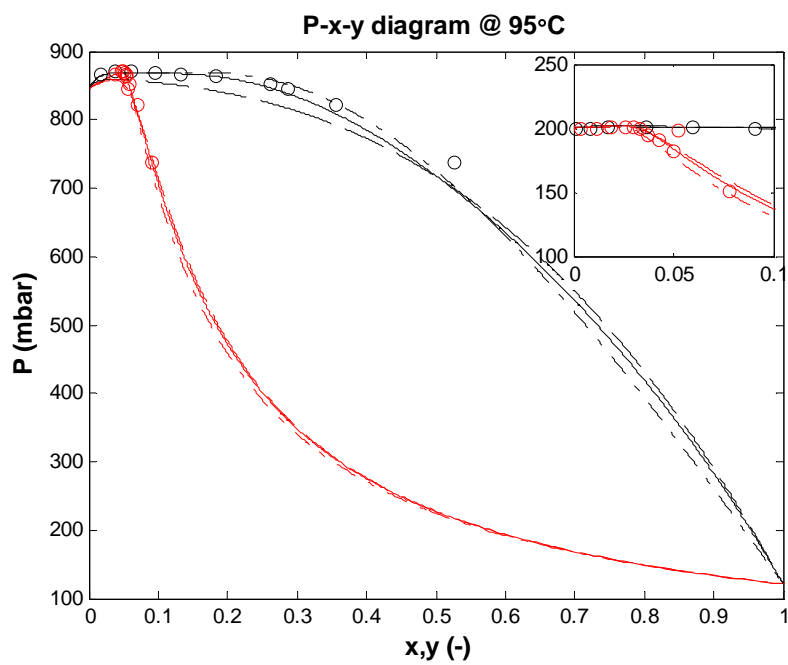
(a)



(b)

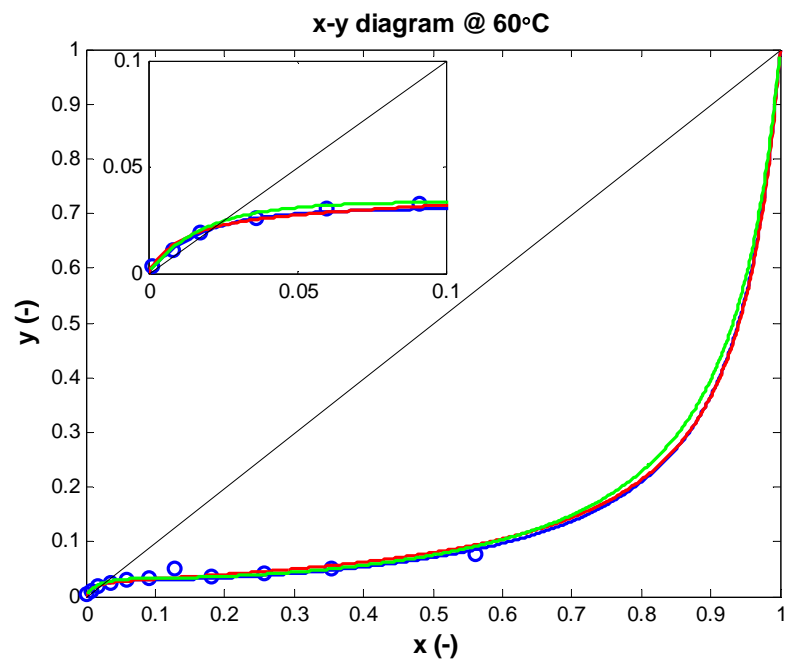
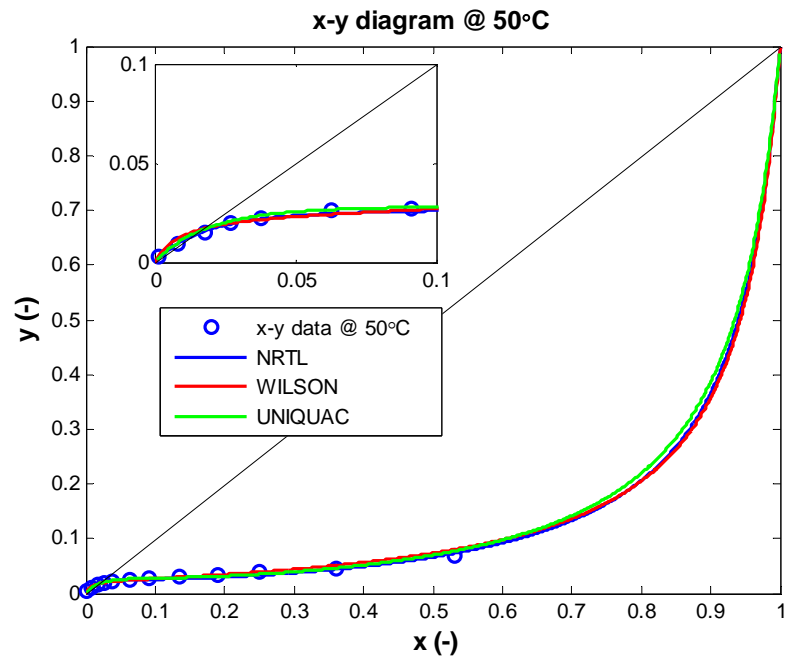


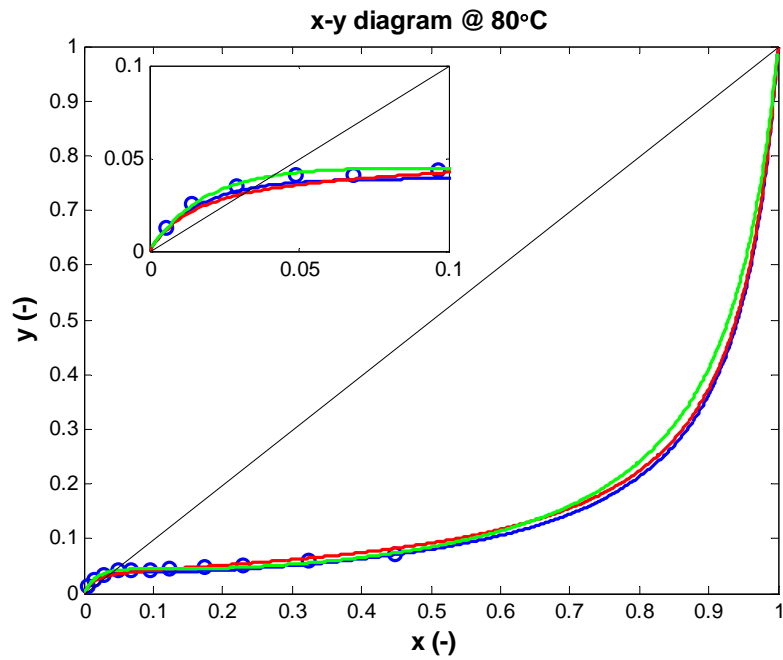
(c)



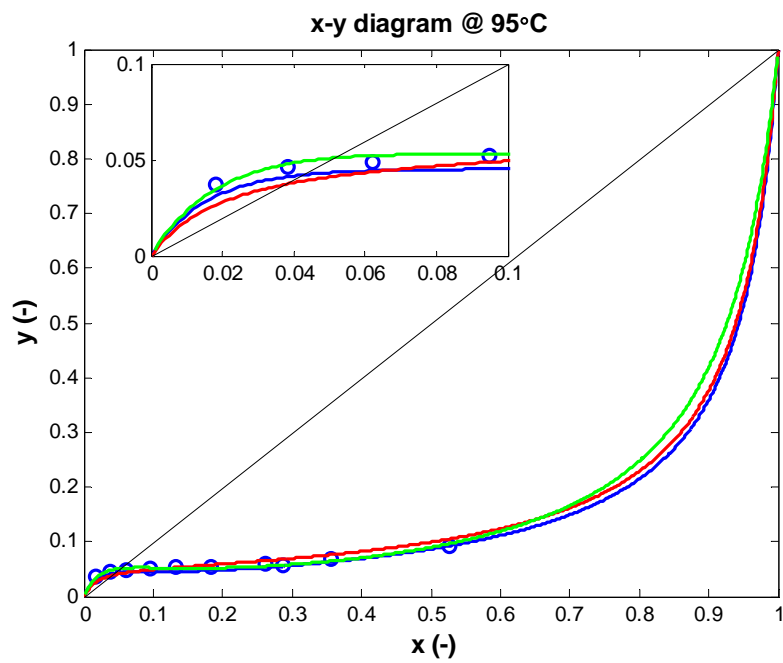
(d)

Figure 3.7: P-x-y plots for DEEA-H₂O system at 50 °C (a), 60 °C (b), 80 °C (c), 95 °C (d), Red=y, Black=x, —, NRTL; ---, Wilson; — • —, UNIQUAC



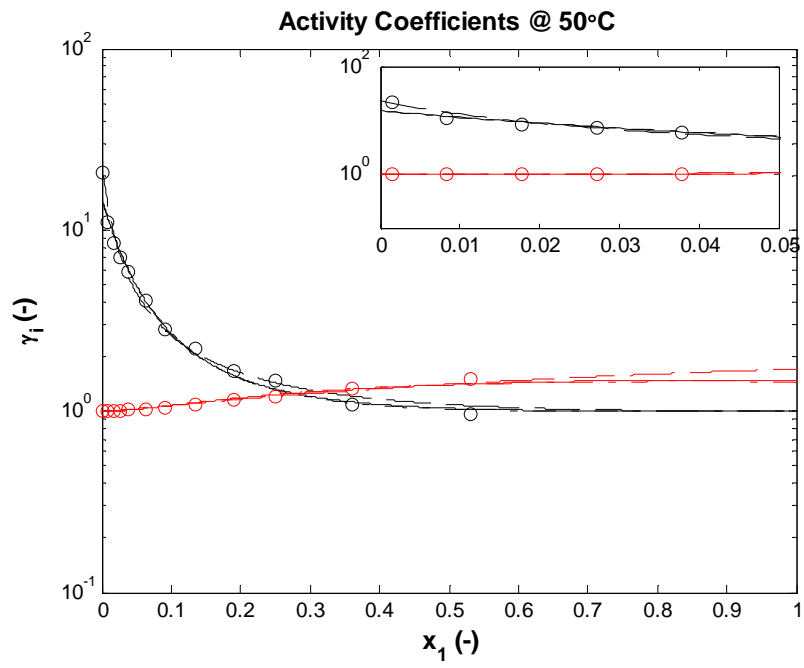


(c)

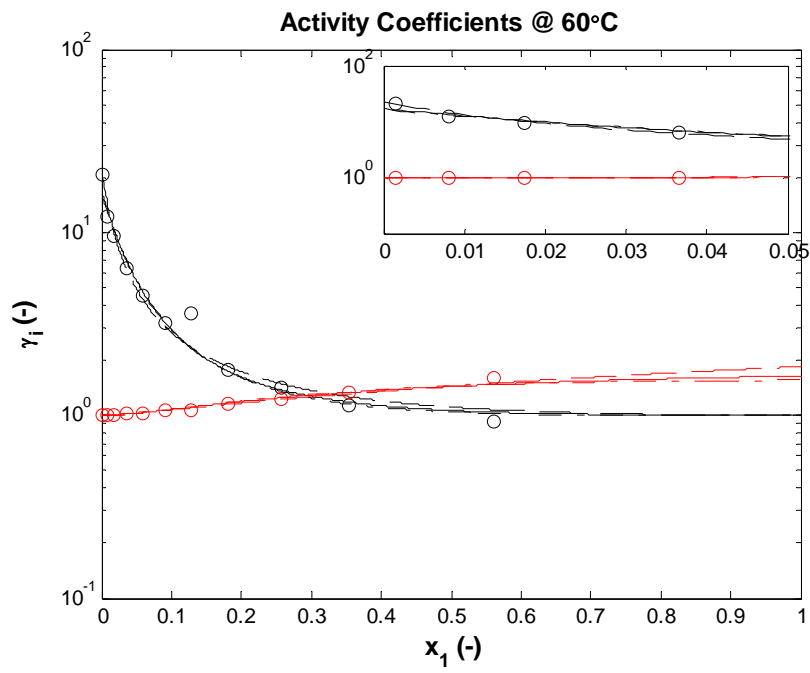


(d)

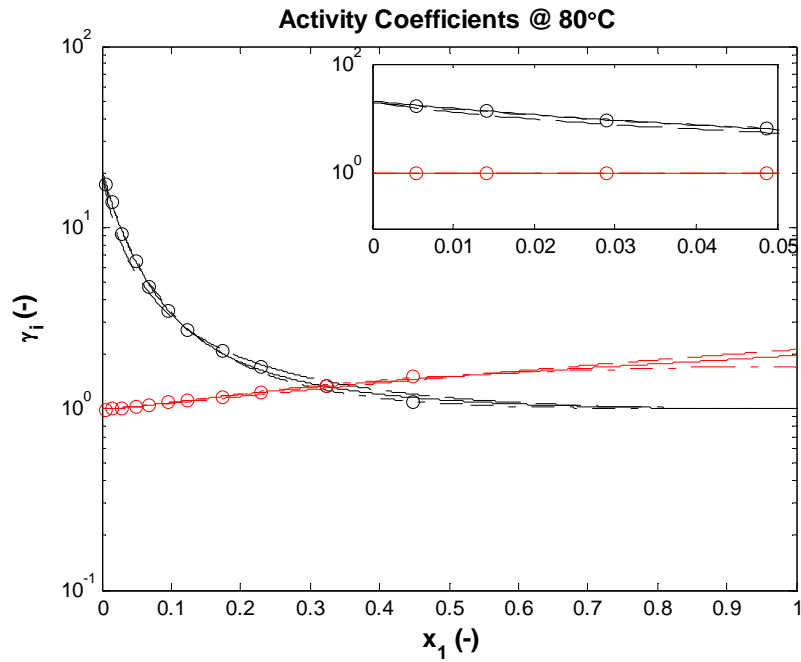
Figure 3.6: x-y plots for DEEA-H₂O system at 50 °C (a), 60 °C (b), 80 °C (c), 95°C (d), with azeotropic region shown in the smaller diagram



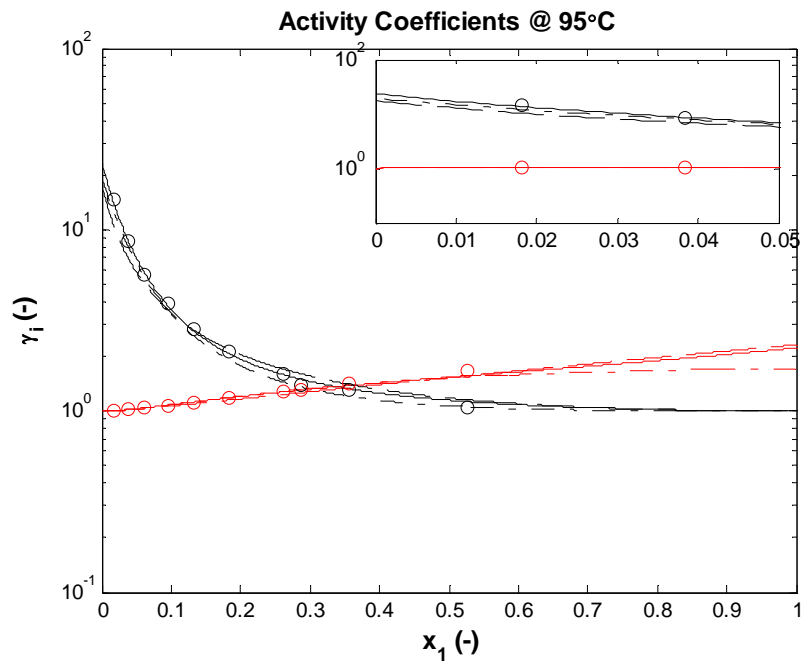
(a)



(b)



(c)



(d)

Figure 3.8 (a, b, c, d): Activity coefficients for DEEA (1)-H₂O (2) system at 50 °C (a), 60 °C (b), 80 °C (c), 95°C (d), Red=H₂O, Black=DEEA, —, NRTL; ---, Wilson; — • —, UNIQUAC

Although all three models seem to fit the experimental data fairly well but based on the rms values associated with all three, it can be said that Wilson and UNIQUAC give very good and comparable results. But looking at the plots one can see that UNIQUAC seems to catch the last point (with lowest concentration) better than the other two.

The best way to check for the thermodynamic consistency of experimental data consists of three steps: First, measure all three quantities P , x and y at constant T ; next, select any two of these measured quantities and predict the third using Gibbs Duhem equation and finally compare the predicted third quantity with the measured one (Prausnitz et al.1999).

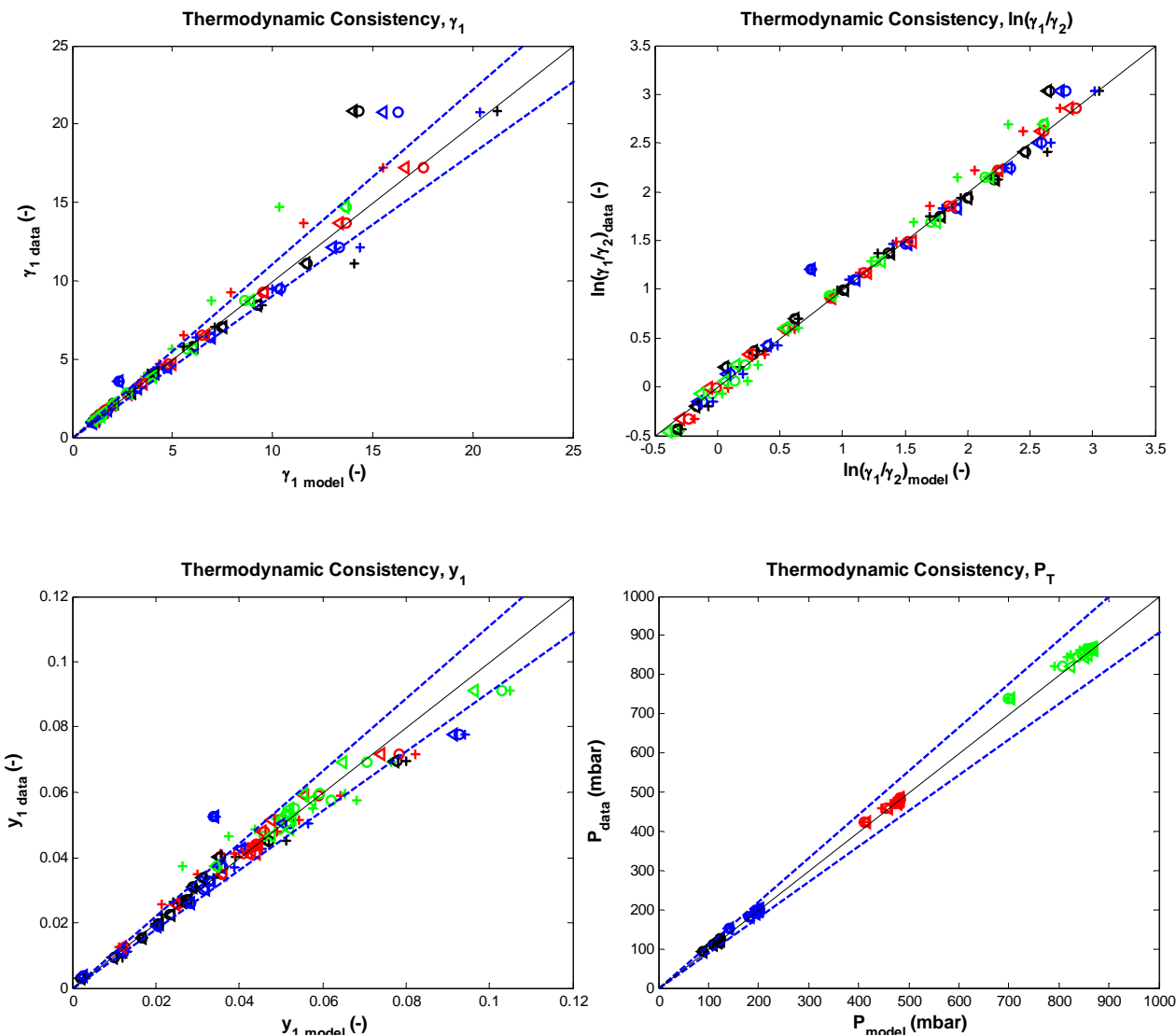


Figure 3.9: Thermodynamic consistency plots. The legend shows the model used with the associated temperature; \circ , NRTL; $+$, Wilson; \triangleleft , UNIQUAC. Colors represent different temperature, Black, 50°C, Blue, 60°C, Red, 80°C, Green, 95°C

Same technique was used in the present work to check the thermodynamic consistency of the experimental data. After observing the above plots it can be said with reasonable certainty that the experimental data obtained in this work is very consistent. Moreover, the heat excess H^E calculated from the present work was compared with that of Mathonat, et al. (1997), which gives a reasonable fit (with a slight shift) thus providing further evidence of consistency of data.

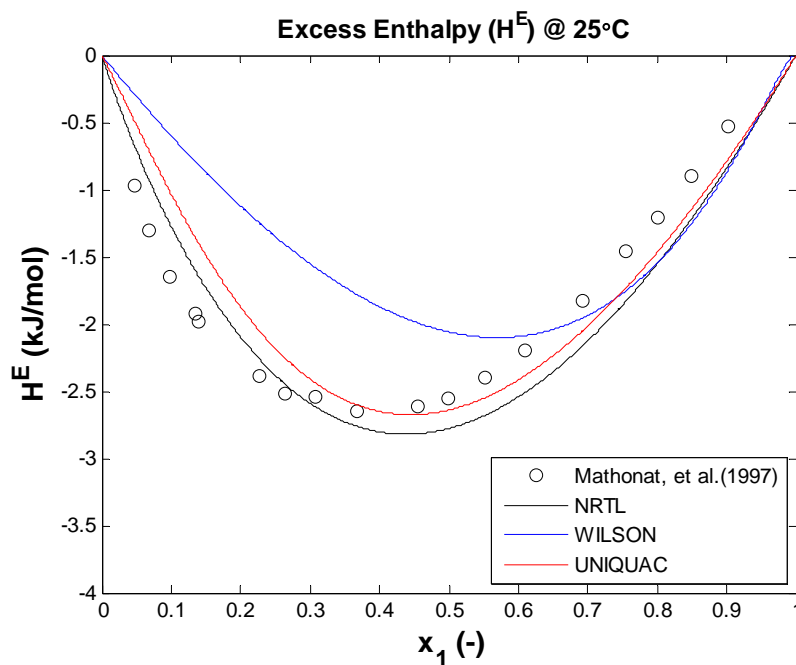


Figure 3.10: Excess enthalpy compared with literature data (at 25°C)

RMS errors were calculated making use of the equation:

$$RMS(\delta y) = \sqrt{\sum_{i=1}^n \frac{(y_i - y_i^{calc})^2}{n}} \quad \delta y = \text{Calculated quantity} - \text{measured quantity}$$

Error	Wilson	NRTL	UNIQUAC
rms ($\delta P/\text{mbar}$)	6.99	11.42	6.21
rms (δy_1)	0.0046	0.0062	0.0043
rms ($\delta \ln(\gamma_1/\gamma_2)$)	0.1155	0.1375	0.1190

Table 3.4: RMS errors for model fitting

The low rms errors obtained from all three models again speak volumes for the accuracy of the experimental data.

Furthermore, a T-x-y diagram was plotted based on the parameters obtained in this work (Table 3.5) and compared with the isobaric experimental data from Dow Chemicals. It provides a very good fit and the extreme points present at the low concentration end gives evidence of azeotrope formation in this region.

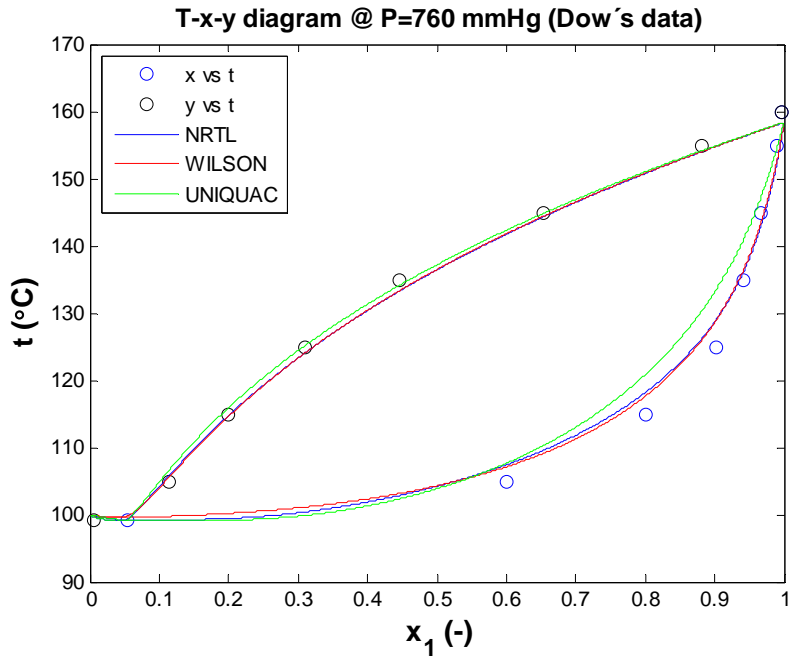


Figure 3.11: T-x-y plot from present work model and the one from DOW

Finally the excess functions (G^E and H^E) for DEEA-H₂O system are presented below, plotted for all three models and all temperatures used during the course of present work. The plots can be a bit uncertain due to lack of data in the higher concentration range.

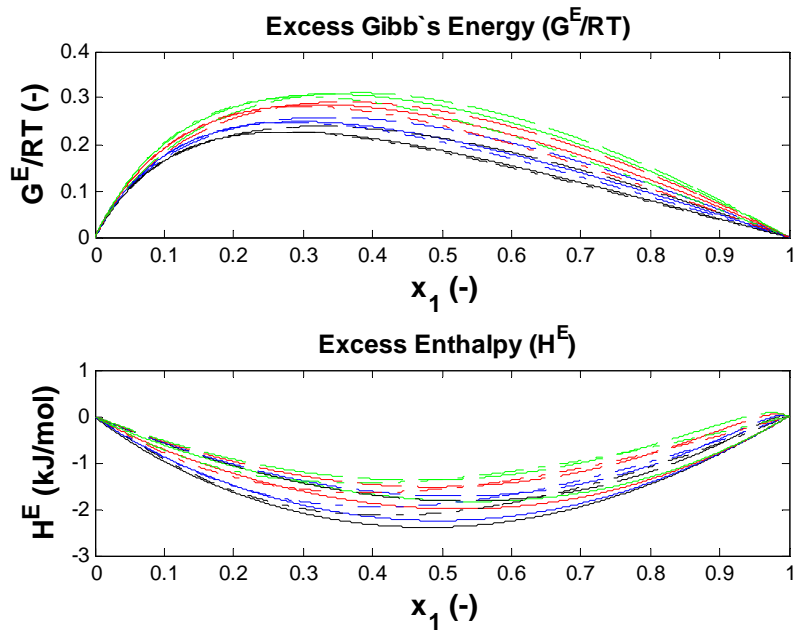


Figure 3.12: Excess functions for DEEA+H₂O system (50-95°C with all three models)

Wilson	
λ_{12}	-6584.4±80
λ_{21}	15393.6±258
NRTL	
a_{12}	3.2798±0.7
b_{12}	-1098.1803±220
a_{21}	3.4561±1
b_{21}	-201.3241±387
$\alpha_{12}-\alpha_{21}$	0.6023±0.1
UNIQUAC	
r_1	5.2472±4
q_1	3.0965±1
u_{ki}^o	$\begin{bmatrix} -246.98 & -259.40 \\ -259.40 & 0 \end{bmatrix}$
u_{ki}^T	$\begin{bmatrix} -4.54 & -1.59 \\ -1.59 & 0 \end{bmatrix}$

Table 3.5: Binary interaction parameters for all the models used in the present work

The parameters for NRTL show larger standard deviation than the other two models but it is well known that parameters of NRTL are often highly co relational. So the poor confidence in NRTL parameters may be explained by a high degree of correlation between the corresponding parameters (Kim, 2009).

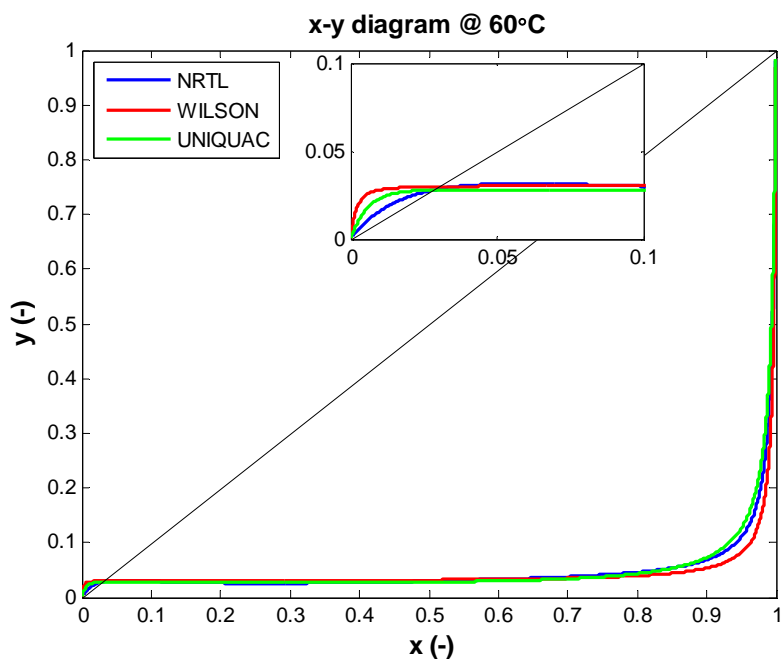
3.9 VLE of DIPEA-H₂O system:

VLE data of DIPEA-H₂O mixture was collected in the same way as that for DEEA-H₂O mixture. The three temperatures for which experiments were carried out were: 60, 80 and 95°C with almost the same concentration range as for DEEA. The main problem encountered during the DIPEA experiments was the immiscibility of DIPEA with water. It was observed that pure DIPEA when added to water forms an emulsion. This phenomenon was observed at all temperatures and concentrations.

As stated earlier, the motivation of this work was to use FTIR as amine analysis technique (especially for vapor phase samples) but the problem of DIPEA's immiscibility with water made it impossible to apply this technique to calculate amine concentration for DIPEA-H₂O mixture. The nonhomogeneity of the samples caused problems with obtaining the expected 'sequential spectra' from the calibration solutions of (gradually) increasing concentrations. This large variation in the spectra rendered The Unscrambler incapable to produce a model which can be deemed good enough to predict the concentrations of the unknown vapor phase samples. Thus after some struggle, efforts to calculate the vapor phase concentration by FTIR were aborted and the following procedure was adopted for this purpose.

According to phase rule P , T and x data is enough to characterize the whole system and based on this data only, y values can be calculated. In such a procedure, total pressures are measured as a function of the liquid phase composition and composition of the vapor phase is calculated from this data with the help of Gibbs Duhem equation (Prausnitz et al. 1999) which is exactly how it was implemented in the present work.

Looking at the x - y and P - x - y plots (see figures below) of DIPEA- H_2O mixture we see that although there is an indication of azeotrope formation at low concentrations but the uncertainty associated with the vapor phase concentrations (which happen to be calculated from Gibbs Duhem equation) and lack of liquid phase data in this range makes it quite uncertain. Also the physical observations made during the experiments themselves don't give any evidence of azeotrope formation. During the experiments it was observed that the two phases are totally immiscible and form emulsion as soon as they are mixed, even in very low concentration. Moreover, it is very difficult to obtain data for this system down to very low concentration because when even very small amount of DIPEA is added to pure water, it causes a lot of variation in the level which makes it impossible to collect the vapor phase samples because of mixing of the liquid phase into the vapor phase sample point. So the concentration had to be increased most of the times (up to ~ 10 wt %) to subside the variation in level before the vapor phase samples could be collected.



(a)

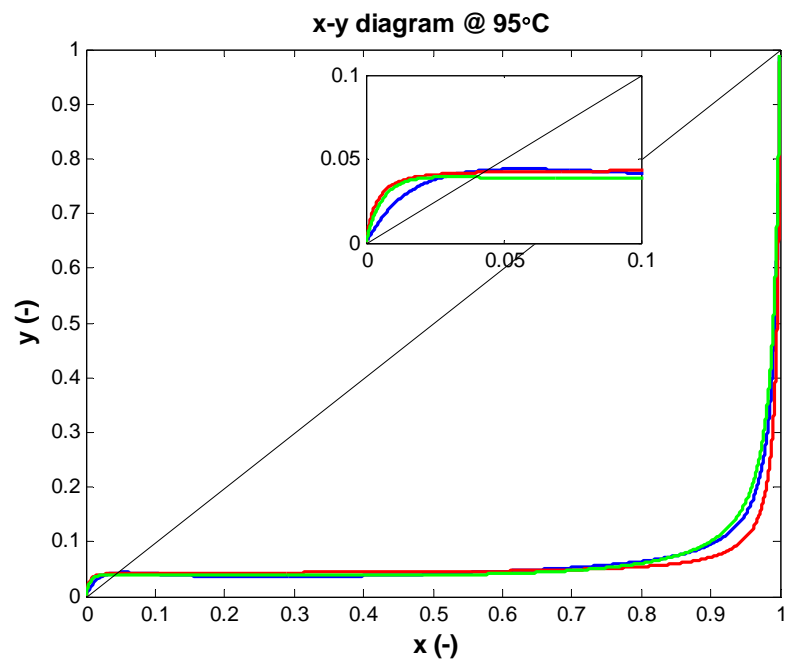
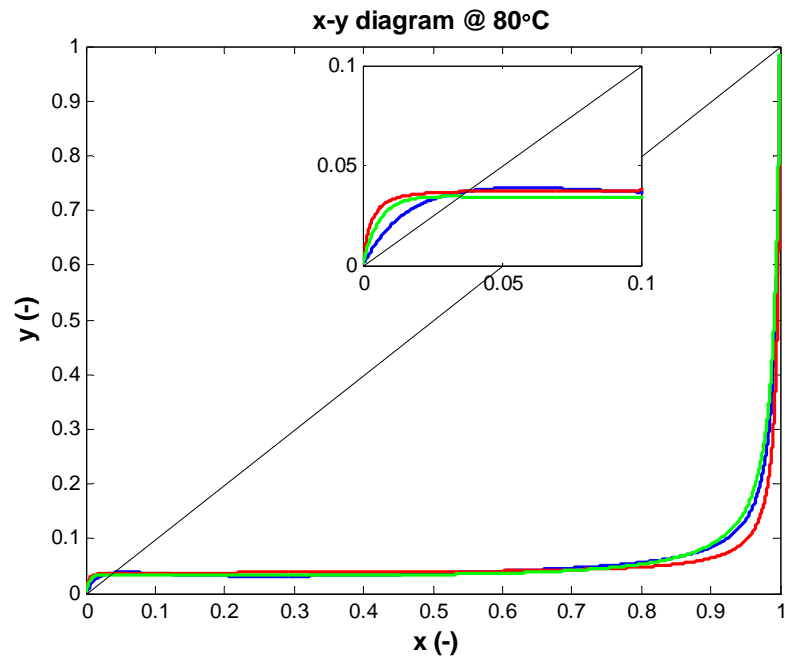
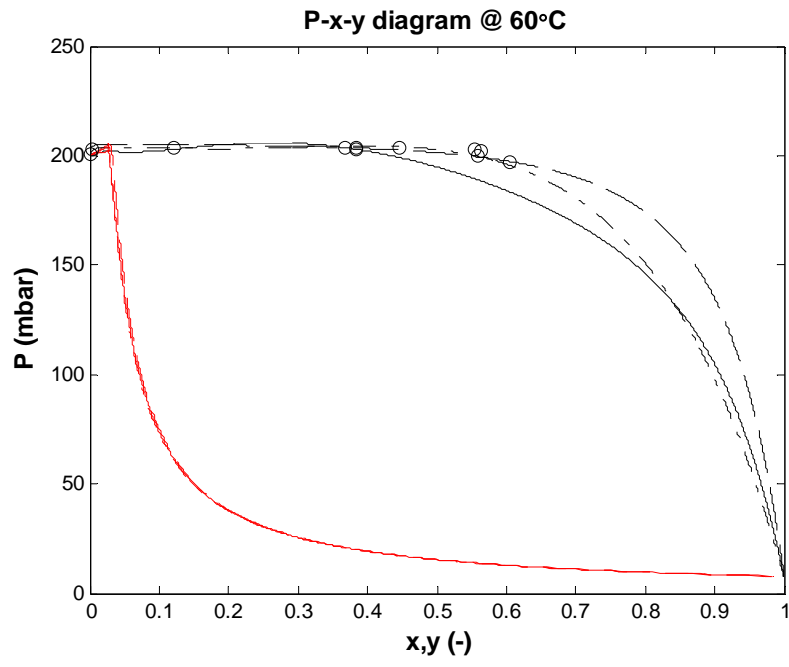
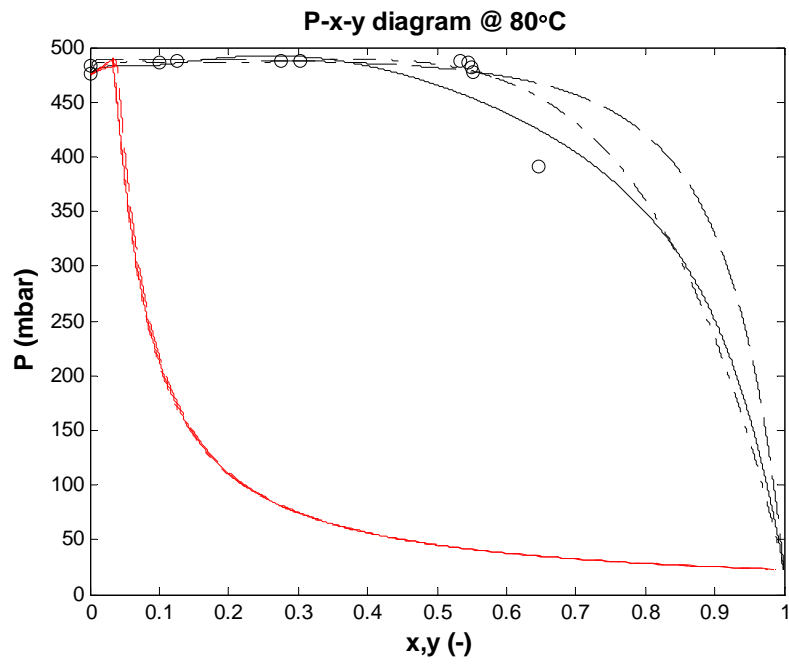


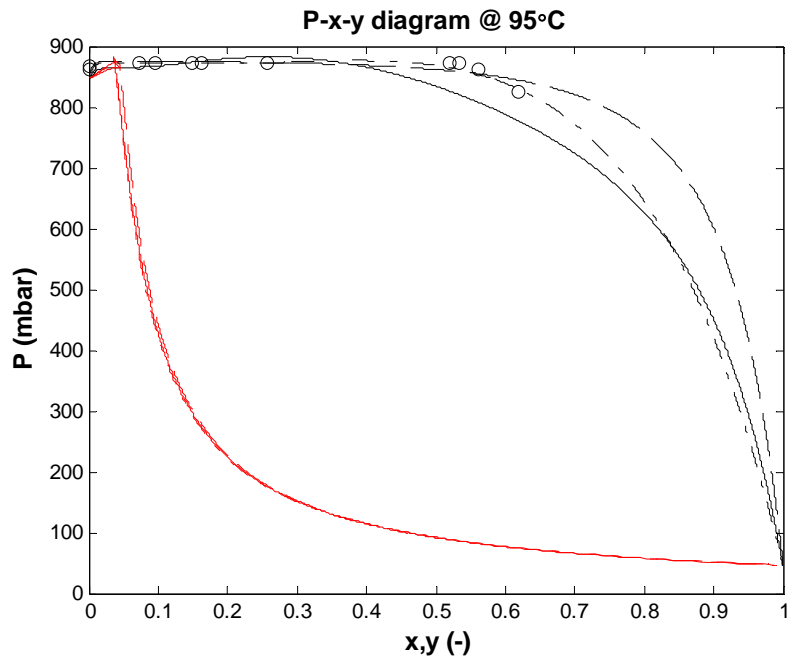
Figure 3.13 (a, b, c): x-y diagram for DIPEA-H₂O system



(a)



(b)



(c)

Figure 3.12: P-x-y diagram for DIPEA-H₂O system at 60 °C (a), 80 °C (b), 95 °C (c), Black=liquid, Red=Vapor, —, NRTL; ---, Wilson; — • —, UNIQUAC

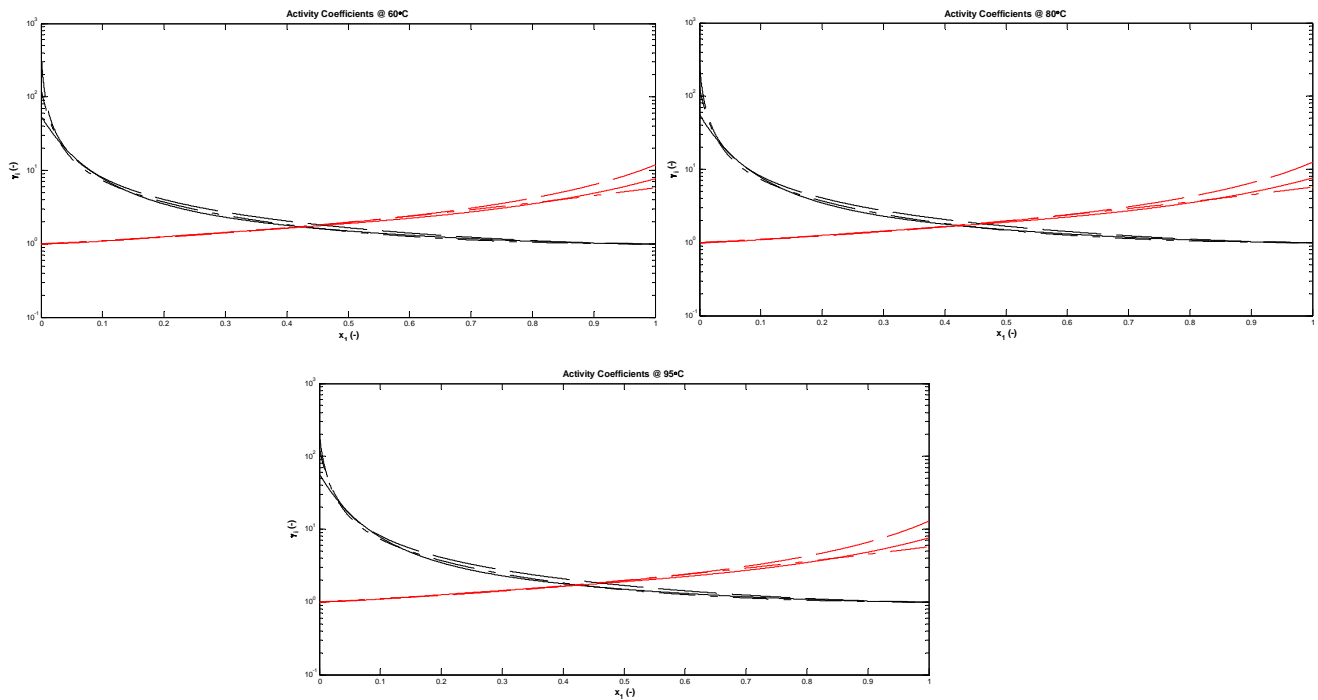


Figure 3.14: Activity coefficients vs liquid phase concentration, Black=DIPEA, Red=H₂O

—, NRTL; ---, Wilson; — • —, UNIQUAC

As shown in figures 3.12, 3.13 & 3.14, all three models (NRTL, Wilson & UNIQUAC) were used in this case also. Lack of data in the lower concentration region makes it difficult to see which model fits better to experimental data (wherever it is available). The table below gives the binary interaction parameters for DIPEA-H₂O system for all three models used during the course of this work.

Wilson	
λ_{12}	-2122.49±258
λ_{21}	20700.98±984
NRTL	
a_{12}	1.1810±0.5
b_{12}	52.9531±174
a_{21}	3.7267±0.7
b_{21}	-145.6672±236
$\alpha_{12}=\alpha_{21}$	0.4705±0.003
UNIQUAC	
r_1	13.3807±3
q_1	12.1369±3
u_{ki}^o	$\begin{bmatrix} -868.24 & -127.12 \\ -127.12 & 0 \end{bmatrix}$
u_{ki}^T	$\begin{bmatrix} -2.62 & 2.24 \\ 2.24 & 0 \end{bmatrix}$

Table 3.6: Binary interaction parameters for all the models used in the present work

Since Gibbs Duhem equation was used to calculate to the y values so thermodynamic consistency of the data could not be tested the way it was done for DEEA-H₂O system where we had an over determined system due to the availability of all P, T, x and y parameters.

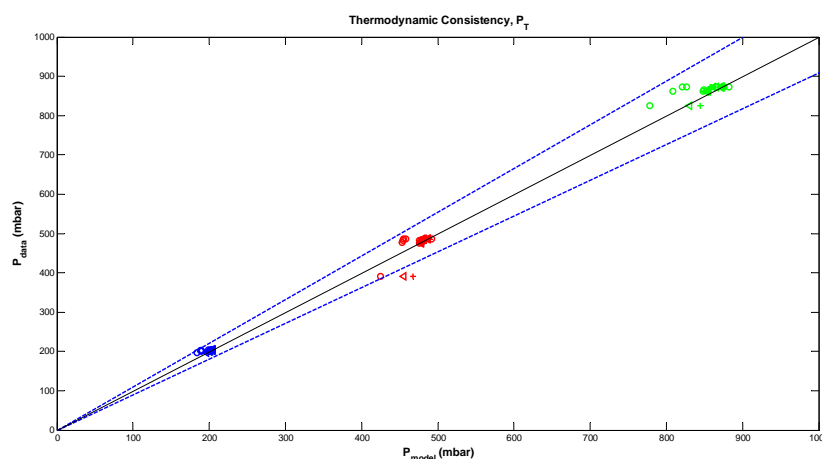


Figure 3.16: Thermodynamic consistency test, Blue, 60°C; Red, 80°C, Green, 95°C, ○, NRTL; +, Wilson, △, UNIQUAC

Error	Wilson	NRTL	UNIQUAC
rms ($\delta P/\text{mbar}$)	80.22	78.99	80.04

The large rms values point to the fact that P, T & x data is not sufficient to ascertain the thermodynamic consistency for the system.

Excess Gibbs energy was also calculated and plotted against liquid phase concentration but the plot is quite uncertain due to the absence of data in the higher concentration region and also it shows the inability of the models to take into full account the temperature dependency of G^E .

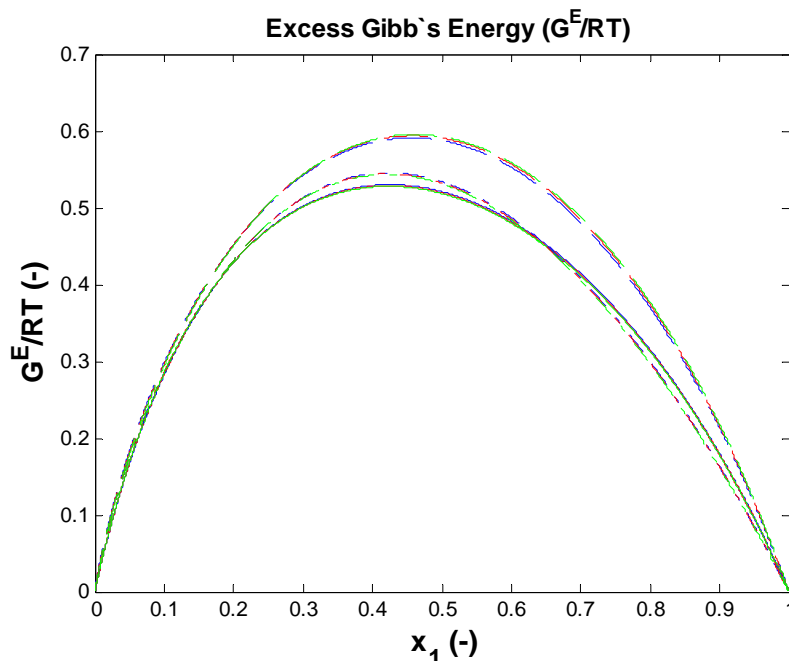


Figure 3.17: Excess Gibbs energy plot DIPEA-H₂O system

3.10 Probable sources of error:

The Świątosławski ebulliometer used in this work is a very accurate apparatus for VLE measurements. The reproducibility of results is very good but the only error which can presumably affect the reproducibility is the very small of residual liquid present in the mixing chamber after every experiment. It is hard to remove it and can cause some variations in repeated results especially if some pure specie is being tested. While testing amine water mixtures the results don't get affected to a large extent but extra care needs to be taken when testing pure species. During the course of this work the ebulliometer was washed twice before starting every new experiment. By wash it is meant that the ebulliometer was filled twice with the desired amine before starting each experiment. But with pure amines' testing the desired amine had to be boiled and discharged many times (3 times for DEEA and 5 times for DIPEA) before good reproducibility of results could be obtained.

Apart from apparatus itself, the other type of errors could have been introduced into the calculations by analyses techniques used for measuring amine concentrations. As described earlier ‘Titration’ and ‘FTIR spectroscopy’ were the two techniques employed for amine analyses in this work. Titration was done twice for each sample and when the error between the two results was less than 1%, the results were deemed acceptable and an average of these two was used for calculation purposes. In case of vapor phase samples (FTIR analyses) only a few of the samples were repeated to check the reproducibility of the result and it turned out to be very good. The main source of uncertainty in the FTIR analyses could be the deviations present in the results when the concentrations are predicted by The Unscrambler. But it was observed that the more the number of (closely ranged) calibration solutions the better the prediction results get. Keeping this in view, the number of calibration solutions was increased in the later stage, which produced great improvement in the initial results but still there is some deviation in The Unscrambler results which could not be fully eliminated even after all the above stated efforts. But the activity coefficient results and the modeling results (of DEEA) show great consistency and are very comparable with the literature values, which in turn, speak for the good quality of FTIR results also. All in all, it can be said with great certainty that FTIR is a very quick and reliable tool for analyses and can be applied effectively to any type of samples. But it doesn’t seem to give good results with emulsions for which some other technique needs to be employed.

3.11 Proposed Future work and recommendations:

- **Ebulliometer:**

Although DEEA-H₂O system produced very good and reliable results but some problems can be seen from the DIPEA-H₂O results. The main problem during this work has been faced with the two phase formation between DIPEA and water which hindered the predetermined procedure of testing vapor phase samples with FTIR. Once the FTIR technique failed for this system, there was not much time left to look for any other technique for the said analyses. But some of the low (DIPEA) concentration range samples were sent to Sintef’s Biolab, the results of which were obtained only towards the end of this work and are given in Appendix 7. These results look quite logical to say the least, so one option to extend the present work could be to get all the vapor phase samples analyzed by LCMS and complete the data but the second option may also be to separate the two liquid phases (both in liquid and vapor phase samples) and then test them individually by FTIR. But the apparatus design doesn’t allow taking samples of both phases at the equilibrium conditions (the apparatus has to be stopped before the samples can be collected). Also large quantities of vapor phase samples will be required for which one needs to wait a lot while sampling. But at least, both these options are possible and can be implemented. Also the two phases themselves need to be looked into further detail to study the immiscibility of DIPEA-H₂O system because it can be of great significance when such a mixture finds its application in industrial environment.

- **FTIR**

The results obtained with FTIR (for DEEA) are very accurate and trustworthy. As described in chapter 2, although both Distilled water and air can be used as backgrounds spectrum when testing samples with FTIR but the results obtained during this work are all based on air background. This was primarily done keeping in view the observation that the spectra obtained with air background don't show any negative peaks and also there is much less noise as compared to DW background spectra. Although it is believed that the type of background should not affect the results much but the noise level in DW spectra may cast some doubts especially if the data is not 'pre treated' before developing the calibration model. Moreover, The Unscrambler models can also be fine tuned further to improve the results.

Conclusion:

During the course of this work, vapor pressure data of pure water, DEEA and DIPEA was measured. The results give good agreement with literature data.

VLE data of DEEA-H₂O and DIPEA-H₂O systems was then obtained at varying concentration and temperature (50-95°C) range. Experimental activity coefficients were calculated using this VLE data. Moreover, FTIR spectroscopy in conjunction with 'The Unscrambler' was used for amine analyses of the experimental samples and results were compared with those of titration and LCMS. The comparisons give clear evidence of the reliability and repeatability of the said technique.

The experimental activity coefficients were also fit to NRTL, Wilson and UNIQUAC equations. DEEA-H₂O data gives a very good fit while DIPEA-H₂O system could not be modeled properly due to the lack of vapor phase data. Recommendations for further work, in case of DIPEA-H₂O system, are also included.

References:

Internet references [i]

[1i] <http://www.bellona.org/factsheets/1191913555.13>, 05.06.2011

[2i] <http://kspark.kaist.ac.kr/Twin%20Paradox/Relativity%20Facts.htm> 05.06.2011

[3i] <http://physics.schooltool.nl/irspectroscopy/method.php> 05.06.2011

Books and literature references:

- International Energy Agency (IEA), CO₂ capture & storage, a key carbon abatement options, OECD/IEA, 2008
- PerkinElmer USA, Technical note; FT-IR spectroscopy
- FLTA2000 series laboratory FT-IR spectrometer's user guide; ABB December 2002
- Thermo Nicolet corporation, 'Introduction to Fourier transform infrared spectroscopy', 2001
- Aslak Einbu, "Documentation and guidelines for FTIR instrument", 2009
- Kim, I, Svendsen, H.F., Børreson E., (2008). Ebulliometric determination of vapor-liquid equilibria for pure water, Monoethanolamine, N-Methyldiethanol amine, 3-(Methylamino)-propylamine, and their binary 7 ternary solutions. *Journal of chemical engineering data*, 53,2521,2531
- Kim, I. (2009). Heat of reaction and VLE of post combustion CO₂ absorbents. Doctoral thesis at NTNU, 2009:50
- Perry R.H., Green, D.W. (1997). Perry's chemical engineering handbook (7th edition), McGraw Hill
- Prausnitz, J.M, Lichtenthaler, R.N., de Azevedo, A.G (1999). Molecular thermodynamics of fluid phase equilibria (3rd ed.), Prentice Hall PRT: New Jersey, 1999.
- Hala, E.; Pick, J.; Fried, V.; Vilim, O. Vapour-liquid equilibrium; Pergamon press: New York, 1958.
- Denis S. Abrams & John M. Prausnitz, (1975), Statistical Thermodynamics of Liquid Mixtures: A New Expression for the Excess Gibbs Energy of Partly or Completely Miscible Systems. *AICHE journal (Vol. 21, No.1)*
- Grant M. Wilson (1963), Vapor-Liquid Equilibrium. XI. A new expression for the excess free energy of mixing
- Dow Chemical (2003), Alkyl Alkanolamines data, Michigan, USA

Appendices

Appendix 1: Comparison of FTIR and titration results for (DEEA) liquid phase samples

Sample	Predicted		Titration		Deviation	Error
	mol/kg	mol frac	mol/kg	mol frac		
AIR_D602	0.415	0.007791	0.433	0.008150	0.027	4.22
AIR_D603	0.871	0.017161	0.888	0.017534	0.027	1.95
AIR_D604	1.585	0.033852	1.688	0.036494	0.033	6.10
AIR_D605	2.440	0.057944	2.496	0.059711	0.038	2.24
AIR_D606	3.299	0.088265	3.368	0.091037	0.035	2.05
AIR_D607	4.159	0.127432	4.173	0.128164	0.031	0.34
AIR_D609	6.518	0.331918	6.663	0.353615	0.058	2.17
AIR_D610	5.820	0.247830	5.905	0.256515	0.042	1.43
AIR_D611	5.021	0.180049	5.032	0.180801	0.036	0.21
D_11	0.300	0.005566	0.295	0.005478	0.105	-1.56
D_12	0.680	0.013125	0.732	0.014204	0.104	7.08
D_13	1.386	0.028925	1.387	0.028949	0.103	0.07
D_14	2.037	0.045950	2.136	0.048769	0.109	4.61
D_15	2.699	0.066343	2.759	0.068357	0.111	2.16
D_16	3.534	0.097946	3.506	0.096735	0.111	-0.81
D_802	6.340	0.307494	6.459	0.323487	0.137	1.83
D_803	5.572	0.224221	5.624	0.228908	0.127	0.92
D_804	4.955	0.175395	4.936	0.174078	0.119	-0.38
D_805	4.107	0.124744	4.096	0.124181	0.117	-0.27
DEEA_953	6.557	0.337599	6.684	0.356922	0.145	1.89
DEEA_954	6.160	0.285051	6.172	0.286483	0.137	0.19
DEEA_955	5.850	0.250874	5.942	0.260483	0.133	1.55
DEEA_956	5.046	0.181844	5.058	0.182676	0.125	0.23
DEEA_957	4.211	0.130169	4.265	0.133062	0.121	1.27
DEEA_958	0.868	0.017096	0.913	0.018079	0.106	4.97
DEEA_959	1.715	0.037198	1.759	0.038354	0.109	2.50
DEEA_9510	2.533	0.060894	2.572	0.062152	0.109	1.52
DEEA_9511	3.476	0.095493	3.463	0.094949	0.115	-0.38
DEEA_501	0.06213	0.001125	0.07993	0.00145	0.109	22.27
DEEA_502	0.381	0.007127	0.4398	0.008277	0.107	13.37
DEEA_503	0.825	0.016174	0.898	0.017745	0.106	8.13
DEEA_504	1.196	0.024426	1.316	0.027244	0.111	9.12
DEEA_505	1.634	0.035101	1.7385	0.037814	0.11	6.01
DEEA_506	2.471	0.058919	2.585	0.062575	0.113	4.41
DEEA_507	3.325	0.089303	3.376	0.091362	0.117	1.51
DEEA_509	6.541	0.335253	6.712	0.361395	0.147	2.54
DEEA_510	5.774	0.243246	5.836	0.249398	0.133	1.05
DEEA_511	5.112	0.186669	5.164	0.190562	0.126	1.01

DEEA_512	4.264	0.133008	4.295	0.134692	0.120	0.72
-----------------	-------	----------	-------	----------	-------	------

Appendix 2: Calibration solutions for DEEA-H₂O system

Sample	Water	DEEA	wt %	DEEA mol frac	Conc mol/kg
	(g)	(g)			
DEEA- C1	49	1	2	0.0031	0.170662
DEEA- C2	48	2	4	0.0064	0.341323
DEEA- C3A	47	3	6	0.0097	0.511985
DEEA- C4A	46	4	8	0.0132	0.682646
DEEA- 5A	45	5	10	0.0168	0.853308
DEEA- C3	45	5	10	0.0168	0.853308
DEEA- C6A	44	6	12	0.0205	1.023969
DEEA- 7A	43	7	14	0.0244	1.194631
DEEA- 8A	42	8	16	0.0284	1.365293
DEEA- 9A	41	9	18	0.0326	1.535954
DEEA- C4	40	10	20	0.0370	1.706616
DEEA- 10A	38	12	24	0.0463	2.047939
DEEA- C5	35	15	30	0.0618	2.559924
DEEA- C6	30	20	40	0.0929	3.413231
DEEA- C7	25	25	50	0.1331	4.266539
DEEA- C8	20	30	60	0.1873	5.119847
DEEA- C9	15	35	70	0.2638	5.973155
DEEA- C10	10	40	80	0.3806	6.826463
DEEA pure					8.571

Appendix 3: Experimental data from pure DEEA and DIPEA (only the best 2 experiments are presented here)

Pure DIPEA				Pure DEEA data			
Experiment 3		Experiment 4		Experiment 1		Experiment 2	
Temp	Pressure	Temp	Pressure	Temp	Pressure	Temp	Pressure
°C	Mbar	°C	Mbar	°C	mbar	°C	
84.942	29.8	84.99	29.8	64.97	29.8	64.91	29.8
90.044	36.8	90.003	36.8	69.7	37.8	70.045	38.8
94.994	45.8	95.019	45.7	74.946	48.8	74.8	48.8
99.987	56.8	100.025	56.8	79.987	61.8	79.842	61.8
105.009	70.8	105.023	70.7	85.001	77.8	84.975	77.8
109.97	86.8	109.993	86.8	90	98.8	89.983	96.8
115.003	107.7	115	106.7	94.97	121.7	95.049	120.8
119.985	130.8	120	129.7	99.996	149.7	99.97	147.8
125	157.7	125.024	156.8	105.035	182.8	105.024	179.8
129.945	189.8	130.007	187.8	109.975	220.8	109.97	216.7
135.004	225.7	134.972	222.8	115.011	265.7	115.016	260.7
139.96	266.8	139.985	264.8	120.005	316.8	120.035	311.8
145.005	315.8	145.008	311.7	125.01	376	124.97	368.9
149.99	369.7	150.008	364.8	130.005	441.8	130	434.9
155.02	429.8	155.004	423.8	134.985	517.9	135.002	509.9
159.993	496.9	159.98	489.8	139.976	603.7	140.013	594.8
165.01	572.8	164.96	563.9	144.986	699.7	144.98	690.1
				150.014	807.8	150.006	796.3
				154.98	926	154.973	914.7

Appendix 4: Experimental data for DEEA-H₂O system

	DEEA	Water		DEEA	Water				
Psat 95	120.8	844.7		Psat 60	22.343	199.46			
Psat 80	61.8	473.9		Psat 50	12.471	123.52			
Sample	Vapor phase			Liquid phase			Total Press	Activity Coefficient	
	DEEA (y ₁)		Water	DEEA (x ₁)		water		DEEA	Water
	mol/kg	mol frac		mol/kg	mol frac		mbar	γ1	γ2
DEEA-Water at 95°C									
D951	3.371	0.091	0.909	7.496	0.526	0.474	737.7	1.058	1.675
D952	2.786	0.069	0.931	6.6835	0.357	0.643	822.7	1.322	1.410
D953	2.426	0.058	0.942	6.172	0.286	0.714	844.1	1.403	1.320
D954	2.492	0.060	0.940	5.942	0.260	0.740	851.2	1.612	1.281
D955	2.345	0.055	0.945	5.0575	0.183	0.817	862.6	2.150	1.181
D956	2.282	0.053	0.947	4.265	0.133	0.867	866.6	2.862	1.121
D957	1.718	0.037	0.963	0.9134	0.018	0.982	866.1	14.783	1.005
D958	2.06	0.047	0.953	1.759	0.038	0.962	870	8.751	1.021
D959	2.132	0.049	0.951	2.572	0.062	0.938	869.7	5.638	1.044
D9510	2.234	0.052	0.948	3.463	0.095	0.905	869.2	3.915	1.078
DEEA-Water at 80°C									
D 11	0.646	0.012	0.988	0.2954	0.005	0.995	473.8	17.389	0.993
D 12	1.24	0.025	0.975	0.73181	0.014	0.986	477.7	13.850	0.997
D 13	1.619	0.035	0.965	1.387	0.029	0.971	480.8	9.330	1.009
D 14	1.865	0.041	0.959	2.1355	0.049	0.951	483.1	6.602	1.028
D 15	1.864	0.041	0.959	2.7585	0.068	0.932	483.8	4.714	1.051
D 16	1.946	0.043	0.957	3.5055	0.097	0.903	482.9	3.506	1.079
D801	2.852	0.072	0.928	7.1785	0.449	0.551	423.9	1.094	1.506
D802	2.468	0.059	0.941	6.4585	0.323	0.677	457.8	1.347	1.344
D803	2.231	0.052	0.948	5.6235	0.229	0.771	471.9	1.720	1.225
D804	2.103	0.048	0.952	4.936	0.174	0.826	476.9	2.120	1.160
D805	1.974	0.044	0.956	4.096	0.124	0.876	479.9	2.763	1.105
DEEA-Water at 60°C									
D601	0.197	0.004	0.996	0.0847	0.002	0.998	199.9	21.046	1.000
D602	0.586	0.011	0.989	0.4333	0.008	0.992	199.8	12.288	0.999
D603	0.945	0.019	0.981	0.88829	0.018	0.982	201	9.630	1.006
D604	1.269	0.026	0.974	1.688	0.036	0.964	201	6.442	1.019
D605	1.437	0.030	0.970	2.496	0.060	0.940	200.3	4.529	1.036
D606	1.544	0.033	0.967	3.368	0.091	0.909	198.9	3.209	1.061
D607	2.261	0.052	0.948	4.173	0.128	0.872	197.8	3.624	1.078
D608	3.025	0.078	0.922	7.617	0.561	0.439	150.9	0.937	1.589
D609	2.187	0.050	0.950	6.6625	0.354	0.646	182.1	1.159	1.341
D610	1.924	0.043	0.957	5.9045	0.257	0.743	190.7	1.424	1.231

D611	1.709	0.037	0.963	5.0315	0.181	0.819	194.8	1.786	1.148
DEEA-Water at 50°C									
D501	0.169	0.003	0.997	0.07993	0.001	0.999	124	21.212	1.002
D502	0.498	0.009	0.991	0.4398	0.008	0.992	124	11.327	1.003
D503	0.785	0.015	0.985	0.898	0.018	0.982	123.8	8.572	1.005
D504	0.983	0.020	0.980	1.316	0.027	0.973	124	7.155	1.012
D505	1.114	0.023	0.977	1.7385	0.038	0.962	124	5.927	1.020
D506	1.273	0.026	0.974	2.585	0.063	0.937	123	4.134	1.034
D507	1.31	0.027	0.973	3.376	0.091	0.909	122	2.902	1.058
D508	2.788	0.069	0.931	7.5115	0.530	0.470	93.8	0.984	1.505
D509	2.011	0.045	0.955	6.7115	0.361	0.639	109.9	1.103	1.330
D510	1.827	0.040	0.960	5.8355	0.249	0.751	115.8	1.495	1.199
D511	1.585	0.034	0.966	5.164	0.191	0.809	119	1.695	1.150
D512	1.477	0.031	0.969	4.295	0.135	0.865	121	2.244	1.097

Appendix 5: Experimental data for DIPEA-H₂O system (The last two columns show the best possible results obtained from FTIR)

Sample	DIPEA conc (Liq)	Total Press	Temp	Vapor phase FTIR results	
	mol/Kg	mbar	°C	Predicted	Deviation
60°C					
DIPAE601	6.368	196.7	60.02	-1.674	1.531
DIPAE602	6.269	199.7	59.951	1.296	1.159
DIPAE603	6.28	201.8	59.974	-0.524	1.348
DIPAE604	6.259	202.8	60.046	1.087	0.905
DIPAE605	5.737	202.8	59.959	1.176	0.913
DIPAE606	5.674	203.9	60.04	1.498	0.826
DIPAE607	0.05598	200.9	59.982	2.933	1.064
DIPAE608	0.15025	202.7	60.007	1.569	0.862
DIPAE609	0.16657	202.9	58.984	2.264	0.856
DIPAE610	3.637	203.8	60.009	3.363	0.94
DIPAE6011	5.743	203.7	60.004	4.11	1.069
DIPAE6012	5.966	203.7	60.005	3.681	1.197
80°C					
DIPEA-801	6.4475	391.8	80.1	3.933	1.41
DIPEA-802	6.257	477	79.975	-22.076	13.768
DIPEA-803	6.2485	482.3	79.97	4.151	1.33
DIPEA-804	6.241	486.2	79.988	4.256	1.31

DIPEA-805	5.1845	486.9	80.039	5.282	1.475
DIPEA-806	5.357	487	80.034	5.132	1.393
DIPEA-807	0.120042	482.6	79.992	5.059	1.528
DIPEA-808	3.2575	486	79.963	4.738	1.591
DIPEA-809	3.6785	486.9	80.012	6.104	1.73
DIPEA-810	6.211	486.9	80.013	6.569	1.885
DIPEA-811	0.0795	476	80.009	6.738	2.11

95°C

DIPEA-951	0.07796	861.9	95.001	6.979	1.954
DIPEA-952	0.099165	866	94.98	6.468	1.984
DIPEA-953	2.642	872.3	95.002	7.041	2.018
DIPEA-954	4.2135	872.5	94.999	6.888	2.148
DIPEA-955	3.1915	872.8	95.002	7.061	2.23
DIPEA-956	4.0125	872.4	95.001	6.983	2.206
DIPEA-957	6.3975	824.8	94.98	8.177	2.367
DIPEA-958	6.274	862	94.99	7.963	2.327
DIPEA-959	6.178	872.9	95.021	7.484	2.27
DIPEA-9610	6.211	872.9	95.013	7.089	2.206
DIPEA-9611	5.0635	873.1	95.012	7.77	2.319

Appendix 6: H₂O vapor pressure data from the present work

Temp		Pressure
°C	K	Mbar
25.237	298.237	32.80
29.91	302.91	42.08
34.96	307.96	56.70
39.97	312.97	73.90
45.05	318.05	96.60
49.993	322.993	123.80
54.994	327.994	157.80
60.033	333.033	199.80
65.035	338.035	250.80
70.006	343.006	311.80
75.02	348.02	385.80
80.023	353.023	473.90
85.009	358.009	577.90
90.015	363.015	700.90
95.016	368.016	844.70
100	373	1011.70

Appendix 7: LCMS results for low concentration DIPEA samples

Sample no	Conc
	mol/l
DIPAE-607	0.434
DIPAE-608	0.772
DIPAE-609	0.873
DIPAE-807	1.199
DIPAE-951	0.807
DIPAE-952	1.181